

# Beyond data: leveraging non-empirical information and expert knowledge in Bayesian model calibration

Sarah A. Vollert<sup>1,2,\*</sup>, Christopher Drovandi<sup>1,2,3</sup>, Cailan Jeynes-Smith<sup>2,4</sup>, Luz V. Pascal<sup>1,2,5</sup>, & Matthew P. Adams<sup>1,2,6</sup>

<sup>1</sup>Centre for Data Science, Queensland University of Technology, Brisbane, Australia.

<sup>2</sup>School of Mathematical Sciences, Queensland University of Technology, Brisbane, Australia.

<sup>3</sup>Centre of Excellence for the Mathematical Analysis of Cellular Systems, Queensland University of Technology, Brisbane, Australia

<sup>4</sup>Department of Paediatrics, The University of Tennessee Health Science Centre, Memphis, United States of America.

<sup>5</sup>Commonwealth Scientific and Industrial Research Organisation, Dutton Park, Brisbane, Australia.

<sup>6</sup>School of Chemical Engineering, The University of Queensland, St Lucia, Australia.

\*Corresponding author. E-mail: sarah.vollert@hdr.qut.edu.au.

**Abstract:** Mathematical models connect theory with the real world through data, enabling us to interpret, understand, and predict complex phenomena. However, scientific knowledge often extends beyond what can be empirically measured, offering valuable insights into complex and uncertain systems. Here, we introduce a statistical framework for calibrating mathematical models using non-empirical information. Through examples in ecology, biology, and medicine, we demonstrate how expert knowledge, scientific theory, and qualitative observations can meaningfully constrain models. In each case, these non-empirical insights guide models toward more realistic dynamics and more informed predictions than empirical data alone could achieve. Now, our understanding of the systems represented by mathematical models is not limited by the data that can be obtained; they instead sit at the edge of scientific understanding.

**Teaser:** Expert knowledge, scientific theory, and observed phenomena can improve predictions and inference via model calibration.

# 1 Introduction

Modelling and simulation are invaluable tools for understanding complex systems across a wide range of disciplines, including biology and medicine (Villaverde and Banga, 2014; Kitano, 2002; Qiao et al., 2024), ecology and environmental sciences (Mouquet et al., 2015; Geary et al., 2020), climate and weather science (Sillmann et al., 2017), social sciences (Bellomo et al., 2013; Holme and Liljeros, 2015), physical sciences (Sundberg, 2012; Wellmann and Caumon, 2018), and engineering (Sinha et al., 2001). Mathematical models – such as differential equation models, or agent-based models – encode system knowledge into mathematical frameworks, enabling scientists to analyse, understand and manage complex systems (Craver, 2006). However, these models become useful only if the values of uncertain parameters lead to realistic model simulations.

Model calibration (also referred to as parameterisation, parameter estimation, inverse problems or inference) is the process of fine-tuning model parameters to maximise the chance that model predictions are aligned with observations of the underlying system (Aster et al., 2018). During model calibration, we adjust parameter values to minimise discrepancies between model simulations and observations, thereby improving predictions (Sisson et al., 2018; McElreath, 2018; Martin et al., 2024). Since model outputs are often highly sensitive to parameter choices (Saltelli et al., 2006), careful calibration is essential for ensuring accurate representations of the system. Additionally, inferred parameter values can enhance our understanding of underlying system mechanisms (McElreath, 2018), making calibration valuable not only for forecasting but also for scientific discovery. Thus, identifying parameter values that match empirical observations is a critical process for model development.

However, for many systems we study, obtaining data for calibration is challenging. While advances in technology and data collection have led to an explosion of available data, many scientific domains still face practical challenges that limit data availability. Data collection can be limited by accessibility (e.g., in deep-sea (Levin et al., 2019), or active volcanoes (Deligne et al., 2018)), large scales (e.g., ecosystem species monitoring; Geary et al. (2020)), or invasiveness (e.g., brain biopsies for disease research; Malone et al. (2015)). Time constraints further complicate data availability, especially if events are rare (e.g., floods; Assumpção et al. (2018)), gradual (e.g., climate change; Karl et al. (1989)) or emerging (e.g., pandemics; Britton and Scalia Tomba (2019)). Moreover, some model outputs are inherently unmeasurable and rely on uncertain proxies, such as subjective quality-of-life indicators (Felce and Perry, 1995). While big data has revolutionised fields where continuous or automated data collection is possible, the data in many critical modelling problems remains low quality, low quantity, or high cost. In these cases, modellers must use what data (if any) they can get. Limited data availability diminishes the precision of model calibration, as there may be a wide range of plausible parameter values consistent with the data, and this high uncertainty in parameter values can propagate through to high uncertainty in model predictions. This is especially problematic if the value of a parameter controlling a positive or negative effect on model behaviour is left highly uninformed (see e.g., Botelho et al. (2025)). The effects of limited data on inferences and predictions can reduce trust in models and their ability to inform, analyse and explore a system (Harper et al., 2021).

Yet, even in the absence of classically observed data, many systems that we model have been extensively studied. This research can yield a wealth of information that may not conform to what we classically think of as data – information such as system understanding, documented phenomena, observational insights, and expert knowledge. As such, here we distinguish two types of information. *Empirically measured information* refers to data obtained through direct measurement or observation using systematic, reproducible, and objective methods, such as data collected from experiments, field studies, and sensor recordings. In contrast, we define *non-empirical information* as any knowledge that can inform or constrain a model’s

outputs but is not directly measured and, therefore, is not classified as empirically measured information (see Table 1 for examples). Beyond specific examples of non-empirical information, such as those in Table 1, expert-elicited knowledge can be obtained for calibration in any well-studied system (Krueger et al., 2012). Experts tend to intimately understand the systems they research. For example, if an expert is shown model predictions, and they can identify areas where the predictions appear “wrong” then this information can be utilised in model calibration as non-empirical information.

In this paper, we develop a comprehensive statistical framework that can simultaneously integrate all kinds of empirical and non-empirical information for model calibration in a statistically rigorous manner. This approach opens up new avenues for model calibration by harnessing the power of often-overlooked non-empirical information – information that is usually not considered as data. To accomplish the calibration of simulation models to both empirical and non-empirical information, we formalise this process in an approximate Bayesian framework. Approximate Bayesian computation (ABC) is a flexible approach for model calibration that matches summaries of the model simulations to that of an empirical dataset (Sisson et al., 2018; Beaumont, 2019; Sunnåker et al., 2013). In the case of non-empirical information, we show that summary statistics of an empirical dataset can be substituted for elicited summary statistics, informed by expert knowledge, observed phenomena, theories or other non-empirical information. While ABC was designed for calibrating models to empirical datasets (Sisson et al., 2018; Sunnåker et al., 2013), and few studies have considered non-empirical constraints (Barnes et al., 2011; Vollert et al., 2025), to the authors’ best knowledge, the present work is the first formal quantitative framework for calibrating models to both. Efficiently obtaining model parameter sets from a combination of any empirical and non-empirical information presents an interesting computational challenge. In response, we used sequential Monte Carlo (SMC) techniques (Del Moral et al., 2006; Chopin, 2002; Drovandi and Pettitt, 2011) to develop a bespoke sampling algorithm that simultaneously combines the empirical data and summary statistics of the non-empirical information in an efficient, robust and flexible manner.

From a Bayesian perspective, our method provides a new way to define informed prior distributions using simulation. Prior elicitation is the process of formally translating expert knowledge into a prior distribution for parameter values, which is crucial for reliable calibration and inference (Mikkola et al., 2024; Banner et al., 2020; Gelman et al., 2017). Our approach offers a generalisable and robust alternative prior elicitation method, enabling the construction of informed prior distributions with the added benefit of flexible parameter dependency structures – a non-trivial task (Gelman et al., 2017; Mikkola et al., 2024).

While the framework we propose presents several statistical advances, we focus on the benefits of these methods for mechanistic modellers. Calibrating models with non-empirical information can ensure that a model used for decision-making or analysis contains the behaviours exhibited in the real system, even if the dataset does not. We present several case studies that illustrate the benefits of integrating non-empirical features into model calibration. Firstly, we calibrate a logistic growth model forecasting coral populations using estimates of recovery time post-disturbance (Case study 1: Logistic coral growth). Then, we calibrate an ecological four-species dynamic population model using both a sparse time-series dataset and principles from theoretical ecology governing the expected equilibrium behaviour of the system (Case study 2: Ecosystem population modelling), demonstrating that ignoring long-standing ecological theory can change the predicted outcomes of conservation and management decisions. Lastly, we calibrate a biochemical network model using the observation that these systems must both respond and adapt to changes in the stimulus (Case study 3: Biochemical adaptation), revealing new insights into the binding affinity of catalysts driving homeostasis, relevant for pathology. Together, these case studies showcase the profound effect of non-empirical information on model predictions, management implications, and system understanding.

Non-empirical information			
Scientific discipline	Original statement	Effect on model calibration	References
Biogeochemistry	Lakes can be either oligotrophic or eutrophic and remain in that state until substantially perturbed.	There should be two alternative stable steady states of the nutrient concentration.	<a href="#">Bhagowati and Ahamad (2019)</a> ; <a href="#">Carpenter et al. (1999)</a>
Biology	Multiple sclerosis exhibits relapsing-remitting symptoms that correspond with lesion development.	Modelled degeneration should oscillate as it progresses.	<a href="#">Confavreux et al. (2000)</a> ; <a href="#">Vélez de Mendizábal et al. (2011)</a>
Climate science	Ice core samples can indicate climatic trends across long periods.	Global energy balance models must reflect observed long-term climatic trends.	<a href="#">Cuffey and Brook (2000)</a> ; <a href="#">Dommenget and Flöter (2011)</a>
Ecology	Introducing pigs to the California Channel Islands led to an increase in golden eagle populations and a decrease in fox populations.	When historical perturbations are simulated, predicted population responses must reflect the observed trends.	<a href="#">Roemer et al. (2002)</a> ; <a href="#">Vollert et al. (2025)</a>
Environmental science	Locals who have experienced a flooding event know which roads were submerged and at what times.	Modelled water depth should align with highly localised information.	<a href="#">Saunders et al. (2025)</a> ; <a href="#">Fava et al. (2019)</a> ; <a href="#">Assumpção et al. (2018)</a>
Epidemiology	Outbreaks of COVID-19 in various countries were typically followed by a second smaller wave of infections due to waning immunity.	There should be two consecutive peaks in infections, where the second is smaller.	<a href="#">Rachel (2024)</a> ; <a href="#">Friston et al. (2020)</a>
Sports science	Athletic performance is limited by what can be physiologically achieved, such as heart rate maxima.	Specific quantities of interest are restricted by physiologically reasonable bounds.	<a href="#">Lundby and Robach (2015)</a> ; <a href="#">Stessens et al. (2024)</a>

Table 1: Examples of non-empirical information that can be used for calibrating models.

## 2 Results

### 2.1 Case study 1: Logistic coral growth

Firstly, we demonstrate our approach with a simple logistic growth example. The logistic growth model is ubiquitous in many areas of ecology, medicine, and biology ([Murray, 2002](#); [Simpson et al., 2022](#)). Here, we will use the logistic growth model to represent the recovery dynamics of coral populations. Using logistic growth, the percentage of coral cover on a reef

can be modelled as

$$\frac{dy}{dt} = ry(t) \left(1 - \frac{y(t)}{K}\right), \quad y(0) = y_0, \quad (1)$$

where  $y$  is the coral cover (% area),  $t$  is the time (years),  $r$  is a growth rate parameter ( $\text{year}^{-1}$ ),  $K$  is the carrying capacity (% area), and  $y_0$  is the initial coral cover (% area). This ordinary differential equation can be solved analytically as

$$y(t) = \frac{Ky_0}{y_0 + (K - y_0)e^{-rt}}. \quad (2)$$

Here, three model parameters may require estimation: the growth rate  $r$ , the maximum coral cover  $K$ , and the initial coral cover  $y_0$ .

Other than time-series data, some information may be available to inform the values of parameters  $r$ ,  $K$  and  $y_0$ . For example, there may be physical restrictions on the carrying capacity  $K$  of coral cover, physiological maxima for coral growth rates  $r$ , and knowledge of post-disturbance coral cover  $y_0$ . We use this information to define the prior distribution for model parameters, which describes the distribution of parameter probabilities before considering the data (e.g.,  $K \sim \mathcal{U}(60\%, 80\%)$ ; see Supplementary Materials Section S.1.1 for more details). However, even after capturing all prior knowledge of these parameters, they can be highly uncertain, and therefore of little value for ecological forecasting (see Figure 1B, grey). In a typical parameterisation framework, time-series data would be used to infer these parameters' values (e.g., Simpson et al. (2022)), yielding a posterior distribution describing the probability of parameters after considering both the prior knowledge and the data. However, there may be no monitoring program on the reef of interest. For instance, the Australian Institute of Marine Science's Long Term Monitoring Program is one of the most comprehensive records of coral status on any reef ecosystem; yet with over 3000 reefs on the Great Barrier Reef in Australia, less than 20% have been surveyed (Australian Institute of Marine Science, 2024). Hence, for the all-too-likely scenario that there is no data on a reef of interest, we instead demonstrate how the model could be calibrated using non-empirical information – specifically, the elicited features of coral population recovery.

### 2.1.1 Expert elicited observations are easily incorporated into model calibration

For this illustrative example, we consider two non-empirical constraints. These constraints help ensure that model predictions do not exhibit behaviours deemed impossible by an expert. Following a disturbance (such as a marine heatwave), an ecologist may expect both slow initial growth of coral populations and full recovery within a specified time frame (see Figure 1A). For example, for this reef it might be estimated that:

1. “Coral cover should be less than 10% within the first 5 years”; and
2. “Coral populations should be fully recovered (within 1% area of carrying capacity) within 50 years.”

These two statements can be expressed in terms of the model parameters  $r$ ,  $K$  and  $y_0$ :

$$y(5) = \frac{Ky_0}{y_0 + (K - y_0)e^{-5r}} \leq 10\%, \quad (3)$$

$$y(50) = \frac{Ky_0}{y_0 + (K - y_0)e^{-50r}} \geq K - 1\%. \quad (4)$$

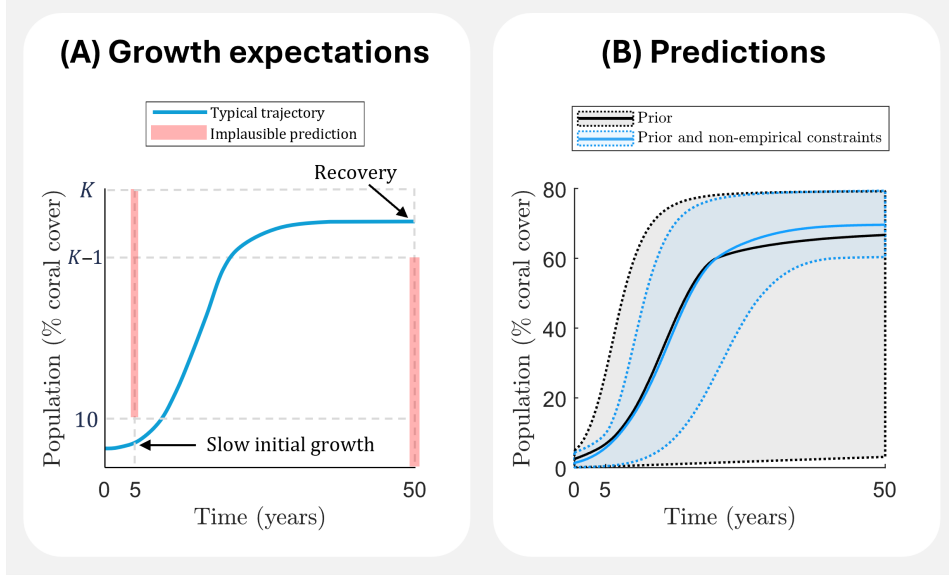


Figure 1: **(A)** Two non-empirical constraints on the growth of coral cover through time. Models predicting this growth should exhibit the two desired behaviours: slow initial growth (coral cover less than 10% at 5 years) and recovery within 50 years (coral cover within 1% area of carrying capacity  $K$ ). **(B)** Model forecasts generated using ensembles of model parameters from both the prior distribution (grey) and the distribution constrained by both the prior and non-empirical sources (blue). Here, the median and 95% credible intervals for predictions are shown as solid lines (black and blue) and shaded regions (grey and light blue) respectively. Models parameterised using both the prior and the non-empirical data sources exhibit the two desired behaviours: slow initial growth and recovery at 50 years. Notice that incorporating these non-empirical constraints significantly shifts the 95% credible interval away from undesirable model behaviours.

However, it is still difficult to directly incorporate these two mathematical statements into the prior distribution. For instance, it would be challenging to describe how the prior distribution for  $K \sim \mathcal{U}(60\%, 80\%)$  should be updated to meet these conditions, both because there are multiple constraints to consider and because there are dependencies between the parameters. Instead, we treat  $y(5)$  and  $y(50)$  as summary statistics and construct non-empirical discrepancy functions  $\rho_5$  and  $\rho_{50}$  that represent the conditions in Equations (3) and (4), which can be calculated for any given values of  $r$ ,  $K$ , and  $y_0$ . These summary statistics can then be easily compared to the behaviours that experts expect via one discrepancy function  $\rho$ :

$$\rho = \rho_5 + \rho_{50}, \quad (5)$$

$$\rho_5 = \max(0, y(5) - 10), \quad (6)$$

$$\rho_{50} = \max(0, K - 1 - y(50)). \quad (7)$$

In Equations (5)-(7),  $\rho_5$  measures the discrepancy of coral cover exceeding 10% in the first 5 years,  $\rho_{50}$  measures the discrepancy of coral cover not recovering within 1% of  $K$  in 50 years, and  $\rho$  measures the total discrepancy between the simulated and expected coral cover.

Using these informative non-empirical constraints together with the less informative prior distribution for parameters  $y_0$ ,  $K$  and  $r$  (Figure 1A), we generated an ensemble of parameter sets yielding model predictions that meet the expected behaviours. The incorporation of expert-elicited observations dramatically shifts the range of model predictions, from highly uncertain (Figure 1B, grey), towards a more constrained range of plausible model behaviours

(Figure 1B, blue). The effect of each of the two individual non-empirical constraints on model predictions can also be clearly identified: the early model predictions are restricted by the slow initial growth constraint, and the predictions beyond five years are controlled by the long-term recovery constraint (Figure S2).

This ensemble generation can proceed via any appropriate ABC sampling algorithm (Sisson et al., 2018), such as rejection sampling, if the non-empirical constraints are not particularly restrictive. However, throughout this work, we instead use an SMC-ABC algorithm (see Supplementary Material S.3 for further details; Drovandi and Pettitt (2011)) as it is an efficient sampling algorithm even when drawing proposals from the prior yields a low acceptance rate. SMC algorithms in general are also particularly robust to multi-modal parameter distributions (Del Moral et al., 2012). In the present work, we will refer to the combination of the prior distribution and *any* constraints (whether non-empirical, a dataset, or both) as the posterior distribution.

### 2.1.2 Incorporating constraints via simulation accounts for parameter interdependencies

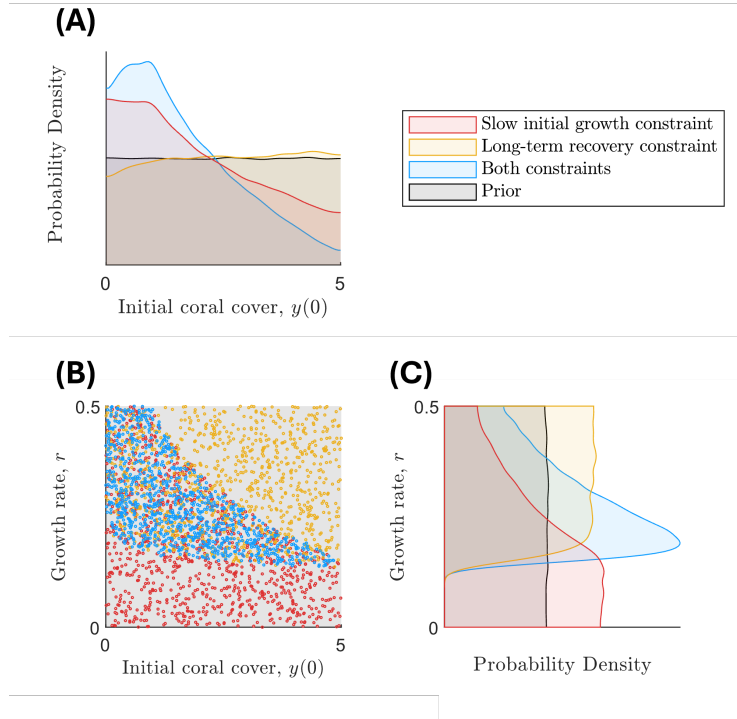


Figure 2: The marginal (A,C) and bivariate (B) parameter distributions for logistic growth model parameters  $y_0$  and  $r$  when sampled from the prior (grey), prior and non-empirical 5-year constraint (red), prior and non-empirical 50-year constraint (yellow), and prior and both non-empirical constraints (blue). This figure shows that the effects of constraints on individual parameters can be obfuscated if parameter interdependencies are not considered. Note that for the parameter  $y_0$  (A), combining the two individual non-empirical constraints (red and yellow) does not yield a joint distribution (blue) between the individual distributions. This counter-intuitive effect can be understood by looking at the joint probability distribution (B) between parameters  $y_0$  and  $r$  obtained via simulation.



From a prior elicitation perspective, we incorporate non-empirical information into the model via simulation because it is challenging to manually update the prior distribution to reflect these constraints. In this case, there are two key reasons that make it difficult to manually define a prior that matches the expert information: (1) the need to satisfy multiple constraints means there can be a trade-off in objectives that changing a parameter value must balance, and (2) mechanistic models create a parameter dependency structure such that parameters need to be jointly considered. Our results demonstrate how these challenges can arise even in this simple three-parameter model.

In this logistic growth model, the value of the initial coral cover parameter  $y_0$  needs to be small to ensure the model exhibits slow initial growth (Figure 2A, red shaded region; Equation (3)), yet long-term recovery is less likely for small initial populations  $y_0$  (Figure 2A, yellow shaded region; Equation (4)). It might be expected that the combination of these constraints will balance the probability distribution of  $y_0$  such that it sits between the two individual constraint distributions. Instead, the initial coral cover  $y_0$  is even more likely to be a small value when both constraints are considered (Figure 2A, blue shaded region) due to compensatory effects with the growth rate parameter  $r$ . Since the growth rate  $r$  must be higher to ensure long-term recovery (Figure 2C), there is less chance that the initial coral cover  $y_0$  can be large and still meet the slow initial growth condition (Figure 2B). Hence, even for a simple three-parameter model, capturing two straightforward constraints (Equations (3) and (4)) yields non-trivial interdependencies between model parameters. Yet, generating the joint parameter distribution that captures these constraints via simulation effortlessly accounts for the model’s parameter dependency structure, which is highly advantageous for prior elicitation.

### 2.1.3 Combining data with non-empirical observations can enhance predictions

While it may be common for a reef of interest to have no monitoring data, roughly 500 out of more than 3000 reefs on the Great Barrier Reef *have* been surveyed ([Australian Institute of Marine Science, 2024](#)), even though only 232 reefs were surveyed more than three times ([Australian Institute of Marine Science, 2015](#)). Hence, we next illustrate the effect of time-series data on model calibration for a hypothetical reef, using three sparse observations of coral cover. For these three data points, we use a Gaussian likelihood function to describe the probability that the model defined by a set of parameters produced the observed dataset (see Methods section 4.3 or Supplementary Material section S.1.1 for more detail). Hence, this model-data fitting exercise accounts for the prior distribution, and the time-series data consisting of three observations simultaneously. We also show the outputs of model-data fitting that accounts for the prior distribution, the time-series data, and the non-empirical constraints simultaneously (Figure 3).



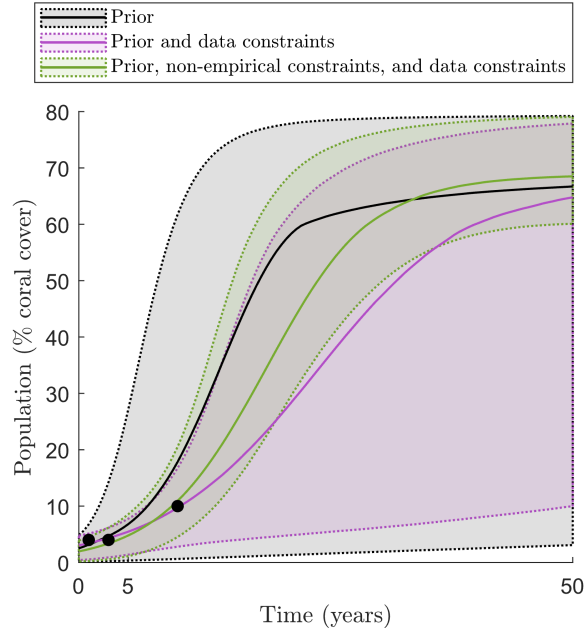


Figure 3: Predictions (median and 95% credible intervals) generated from a prior distribution (grey), a posterior distribution constrained using the dataset (purple), and a posterior distribution constrained using data and non-empirical information, i.e. Equations (3) and (4) (green). Notice that both informed distributions (purple and green) match the dataset, but the one that is additionally constrained by non-empirical information (green) also meets the requirement for recovery within 50 years.

Combining limited data with non-empirical observations leads to model outputs that match both the data and the expert beliefs (Figure 3, green). Calibrating the model to the dataset (Figure 3, purple) can constrain the predictions to a more sensible domain in comparison to the prior distribution (Figure 3, grey). However, this posterior still allows model predictions that exhibit very little recovery in coral cover, which conflicts with the expert belief that coral cover must be within 1% area of carrying capacity after 50 years. Instead, if the model is constrained also by the two non-empirical constraints that represent the expert beliefs (Section 2.1.1), the parameter inferences (Figure S3) and model outputs (Figure 3) satisfactorily match both the expert-informed requirements and the dataset.

## 2.2 Case study 2: Ecosystem population modelling

Ecosystem network models describe the interactions between species and simulate the dynamics of ecosystem populations over time. Ecosystem network models can provide broad insights into how all ecosystems function (Allesina and Tang, 2012; Grilli et al., 2017; Landi et al., 2018) and forecast the potential effects of human impacts and conservation management on specific ecosystems of interest (Baker et al., 2019, 2017; Adams et al., 2020). These ecosystem network models can be calibrated to match any available time-series data from ecological monitoring programs for a specific ecosystem (Adams et al., 2020; Baker et al., 2019). In addition, ecological theory suggests that the equilibrium species populations stably coexist in general (Cuddington, 2001; Allesina and Tang, 2012; Rohr et al., 2014; Grilli et al., 2017; Dougoud et al., 2018; Landi et al., 2018); in other words, species populations can fluctuate over the short-term, but have stable long-term dynamics. Consequently, ecosys-

tem network models for a specific ecosystem are often parameterised under the assumption that they exhibit a stable, coexisting equilibrium (Baker et al., 2017; Rendall et al., 2021; Pesendorfer et al., 2018; Peterson and Bode, 2021; Peterson et al., 2021; Bode et al., 2017).

Approximate Bayesian methods have been previously used to parameterise theoretical beliefs about ecosystem equilibria (Baker et al., 2017; Vollert et al., 2024; Pascal et al., 2025), and a larger variety of methods have been used to calibrate these models to time-series data (Baker et al., 2019; Botelho et al., 2025) including SMC algorithms (Adams et al., 2020). Previously, when equilibrium constraints and time-series data have both been fitted to ecosystem network models, the parameter space was searched using an ad-hoc method similar to SMC-ABC with iteratively introduced dynamic constraints underpinned by a distance measure (Baker et al., 2019). Here, we provide a robust and efficient method for calibrating ecosystem network models using equilibrium constraints and time-series datasets via our combined SMC algorithm (see Supplementary Material section S.3 for more detail).

In this case study, we consider a well-known four-species ecosystem network motif (Monsalve-Bravo et al., 2022; Pech and Hood, 1998) comprised of foxes ( $F$ ), rabbits ( $R$ ), small mammals ( $M$ ) and vegetation ( $V$ ), as depicted in Figure 4A. Using the ubiquitous Lotka-Volterra equations (see e.g., Adams et al. (2020); Baker et al. (2017)), we converted this ecosystem network into a system of ordinary differential equations for calibration.

Firstly, we consider two non-empirical observations from ecological theory that describe the long-term behaviours of ecosystem populations: coexistence and stability. *Coexistence* (often referred to as feasibility) specifically requires equilibrium populations for all species ( $n_F^*$ ,  $n_R^*$ ,  $n_M^*$ , and  $n_V^*$ ) to be positive (Grilli et al., 2017). *Stability* is the ability of ecosystem populations to resist changes from small external pressures (Allesina and Tang, 2012), such that the real parts of all eigenvalues of the Jacobian matrix evaluated at equilibrium ( $\mathbb{R}(\lambda_1)$ ,  $\mathbb{R}(\lambda_2)$ ,  $\mathbb{R}(\lambda_3)$ , and  $\mathbb{R}(\lambda_4)$ ) must be negative (see Vollert et al. (2024) for further details). For this four-species ecosystem network model, all eight summary statistics (four equilibrium abundances  $n_F^*$ ,  $n_R^*$ ,  $n_M^*$ , and  $n_V^*$ , and four real components of eigenvalues  $\mathbb{R}(\lambda_1)$ ,  $\mathbb{R}(\lambda_2)$ ,  $\mathbb{R}(\lambda_3)$ , and  $\mathbb{R}(\lambda_4)$ ) are combined within a single discrepancy function  $\rho$ , calculated as

$$\rho = \sum_{i=\{F,R,M,V\}} |\min\{0, n_i^*\}| + \sum_{j=1}^4 |\max\{0, \mathbb{R}(\lambda_j)\}|, \quad (8)$$

where  $\rho$  measures the discrepancy in equilibrium behaviour from the theorised coexisting and stable behaviour (Vollert et al., 2025).

In addition, we used simulated time-series data for model calibration, where each species has yearly abundance estimates. We used a Gaussian likelihood function which assumes normally distributed measurement noise to match the ecosystem network model’s population prediction to the time-series data. Further detail on the model, prior distribution, summary statistics, and likelihood can be found in Supplementary Material section S.1.2.

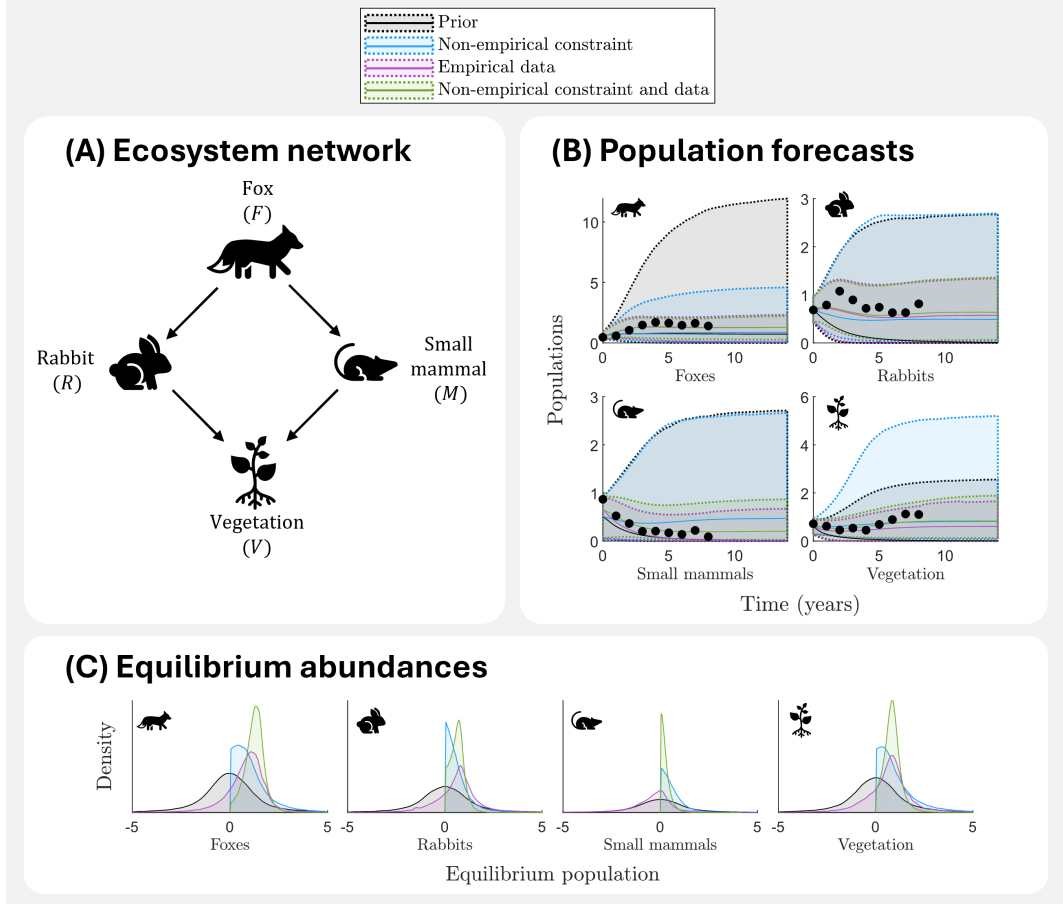


Figure 4: **(A)** Ecosystem network diagram where the arrows indicate the direction of the energy transfer associated with the species interaction due to predation or herbivory. **(B)** Predictions (median and 95% credible intervals) generated from four distributions: the prior (grey), equilibrium-constrained posterior (blue), time-series data posterior (purple) and the combined equilibrium-constrained and time-series data posterior (green). **(C)** Equilibrium populations for each species when calculated using parameter sets from each of the four distributions: the prior (grey), equilibrium-constrained posterior (blue), time-series data-informed posterior (purple), and the combined equilibrium-constrained and time-series data-informed posterior (green). Note, negative equilibrium abundances for a species do not imply that the specific species will go extinct, and instead suggest that not all species can coexist.

### 2.2.1 Non-empirical constraints can ensure long-term model behaviours are theoretically sound

We generated an ensemble of 100,000 parameter sets for the non-empirical equilibrium constraints using SMC-ABC (see [Vollert et al. \(2024\)](#)), for the simulated time-series data using SMC (see [Adams et al. \(2020\)](#)), and for both simultaneously using our combined SMC algorithm (see Supplementary Material S.3; marginal parameter distributions shown in Figure S4). Calibrating the model to the time-series data hones the predictions onto appropriate population sizes, and ensures that the trends in the data are captured (Figure 4B, purple). The long-term non-empirical constraints are required to ensure that the system's equilibrium matches the ecological theory (Figure 4C, blue; Figure S5).

The combination of these two information sources (time-series data and non-empirical constraints) leads to models that both match the dataset well (Figure 4B, green) and exhibit the expected long-term behaviours (Figure 4C, green; Figure S5). However, both sources of information individually fail to capture important aspects of the population dynamics. Using the equilibrium constraints alone fails to capture population sizes and trends clearly seen from the dataset in Figure 4B (blue). Similarly, using the data alone means that there is no knowledge placed into the model indicating how long-term and stable these population fluctuations are, such that the data leads to systems with negative equilibrium abundances (Figure 4C, purple) and instability (Figure S5).

### 2.2.2 Non-empirical information can alter forecasted ecosystem responses to management

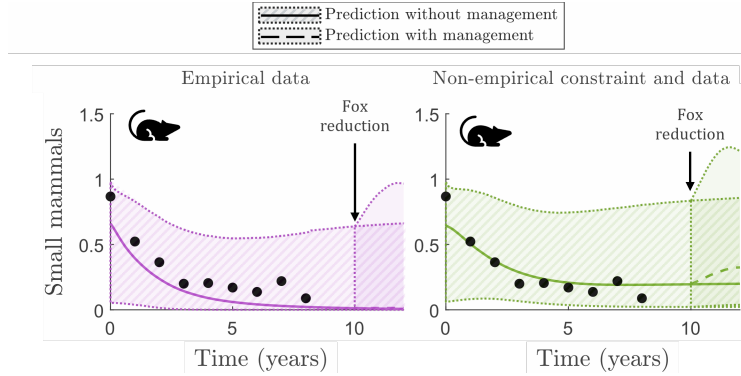


Figure 5: Predicted populations of small mammals, with and without regulating fox populations, across two parameter distributions: the distribution constrained by data (purple), and the distribution constrained by coexistence, stability and data (green). Notice that the constraints on coexistence and stability are necessary for reducing predictions that lead to small mammal extinction.

Incorporating coexistence and stability requirements can cause fundamental differences in the long-term behaviour of the system, and can have major implications for ecosystem management. For a final ecosystem network scenario, we model the effects of reducing fox populations to 20% of their predicted population after 10 years, and analyse the consequences for small mammal populations. Fitting a model to time-series data, without coexistence or stability requirements, yields predictions of the small mammal population heading towards extinction without fox control, and that heavily regulating the predator species, foxes, will also have minimal effect on small mammals (Figure 5, purple).

Contrastingly, also fitting the model to coexistence and stability requirements informs the model that all four species' populations in the network are long-lasting despite their fluctuations. As a surprising consequence, the effects of regulating foxes are much more pronounced and suggest that small mammal populations will recover more strongly in response to this management action (Figure 5, green). Interestingly, in this case, fitting the model to both the non-empirical constraints and the dataset leads to a better match between the median of the model-data fit and the time-series data for the small mammal's population (Figure 5, green), compared to a model fit to the time-series data alone (Figure 5, purple). Whilst we do not expect this improvement in model-data fit due to other constraints to hold in general, it is additional evidence that non-empirical information can have pronounced and unexpected consequences on model predictions.

### 2.3 Case study 3: Biochemical adaptation

A large body of literature utilises mathematical data-free techniques – topological, analytical and numerical methods – to identify biochemical systems that are capable of regulating and adapting to change (Ma et al., 2009; Jeynes-Smith and Araujo, 2023; Araujo and Liotta, 2018; Khammash, 2021; Ferrell, 2016). Biochemical adaptation, or homeostasis, is a fundamental biological feature in which a system is able to repeatedly adapt to changes in a stimulus (Ma et al., 2009; Araujo and Liotta, 2018, 2023; Khammash, 2021); see Figure 6B). However, analytical and topological approaches require strict assumptions yielding mathematical idealisations that are unlikely to occur in real systems (Ferrell, 2016; Aoki et al., 2019; Briat et al., 2016), such as requiring a system to perfectly return to its baseline, and allowing adaptation to occur on infinite timescales (Araujo and Liotta, 2018, 2023; Khammash, 2021; Karp et al., 2012). Hence, numerical methods provide the best path for realistically representing the process of homeostasis in chemical reaction networks, where data is unavailable.

In the field of biochemical adaptation, accept-reject methods for identifying homeostasis face a computational bottleneck that limits the size and consequently representativeness of the obtained ensemble of adaptation-capable parameter sets; for example, the seminal work of Ma et al. (2009) found that 1 in 10000 (0.01%) tested parameterisations were capable of adaptation (Jeynes-Smith and Araujo (2023) and Skataric and Sontag (2012) report similar rates). To account for this problem, extended analyses of adaptation have often relied on reducing the parameter space being considered (Ma et al., 2009) and separately manipulating subsets of parameters (Jeynes-Smith and Araujo, 2023). However, these studies struggle to obtain a large and representative sample of parameter sets that lead to biochemical adaptation.

An example of biochemical adaptation is seen in chemical reaction networks, such as the one depicted in Figure 6A, that consist of a system of interacting proteins ( $A, B$ ), enzymes ( $E_1, E_4$ ) and complexes ( $C_1, C_2, C_3, C_4$ ), typically represented as a system of ordinary differential equations (Ma et al., 2009; Jeynes-Smith and Araujo, 2023). For this case study, we use a general modelling framework known as ‘complex complete’ (Jeynes-Smith and Araujo, 2023) which explicitly accounts for the intermediate formation of complexes (the combination of enzymes and substrates) at the expense of additional parameters. This model consists of ten ordinary differential equations, and twelve highly uncertain reaction rate parameters that are typically drawn from independent log-uniform distributions spanning several orders of magnitude (Jeynes-Smith and Araujo (2023); see Supplementary Materials Section S.1.3 for more detail). Under some specific parameter combinations, the network depicted in Figure 6A can adapt to changes in input. To simulate this model for any given parameter set, the steady state is first numerically obtained, the input is changed (a process called “stimulation”), and the model is solved under these new conditions to assess whether it returns to the same steady state or not (Figure 6B).

The system is considered adaptive if it meets two conditions after the input is changed: it must be sufficiently *sensitive* and sufficiently *precise* (Ma et al., 2009). Sensitivity,  $S$ , measures the ability of a chemical concentration,  $O$ , to react to a change in input,  $I$ ,

$$S = \frac{|O_{\text{peak}} - O_1|/O_1}{|I_2 - I_1|/I_1}, \quad (9)$$

where  $O_1$  and  $I_1$  are the original chemical concentrations of the output and input at steady-state, respectively,  $I_2$  is the updated input after stimulation, and  $O_{\text{peak}}$  is the concentration of  $O$  which is furthest from  $O_1$  after stimulation (see Figure 6B). A biochemical network that is sufficiently sensitive to changes in input will have  $S > 1$  (Ma et al., 2009).

The precision,  $P$ , is a measure of how well the system can return to its original value,

$$P = \left( \frac{|O_2 - O_1|/O_1}{|I_2 - I_1|/I_1} \right)^{-1}, \quad (10)$$

where  $O_2$  is the final output after the input changes. A biochemical network is considered precise if  $P > 10$  (Ma et al., 2009). Hence, we can utilise these two summary statistics (sensitivity and precision) to define a measure of discrepancy  $\rho$  between adaptive biochemical networks and a model simulation as

$$\rho = \max(0, 1 - S) + \max(0, 10 - P), \quad (11)$$

such that  $\rho$  measures the discrepancy from a sufficiently sensitive and precise system. Further details on the model, prior distribution, summary statistics, discrepancy, and likelihood can be found in the Supplementary Material Section S.1.3.

### 2.3.1 Models can still be calibrated even without empirical data

Using SMC-ABC with these summary statistics and discrepancy function, we produced an ensemble of 10,000 parameter sets that led to adaptation in this network. In comparison to simulations from the prior distribution, simulations from the posterior show the output is both sensitive to stimulation and precisely able to return to pre-stimulation levels (see Figure 6C, Figure 6E)).

### 2.3.2 Deeper insight can be gained by using statistically robust methods to thoroughly search the parameter space

An ensemble of parameter sets capable of adaptation (see Figure 6D for parameter distributions) can be used to test interventions or analyse the network conditions that lead to the adaptive capability (Jeynes-Smith and Araujo, 2023). Using a simplified modelling framework applied to the network in Figure 6A, Ma et al. (2009) analytically showed that adaptation could only be achieved when the parameter combinations  $K_3 = \frac{d_3+k_3}{a_3}$  and  $K_4 = \frac{d_4+k_4}{a_4}$  were significantly smaller than 1. While we generally observe this result within our parameter sets (Figure 7, univariate distributions), our results numerically show that this condition is not strictly necessary for adaptation, and the bivariate distribution of these quantities of interest suggests that there may be some relationship between  $K_3$  and  $K_4$  (Figure 7, bivariate distribution).

This relationship may not have previously been uncovered because previous parameter searches have been more coarse (testing fewer parameter sets in the space) and have considered a smaller parameter space due to the low probability of identifying adaptation and the computational challenges of simulating these systems. For example, Jeynes-Smith and Araujo (2023) limited their search to a few orders of magnitude and held select parameters constant to explore the effects of stimulation range. Parameter sets that fall outside the area identified by the literature still display adaptive trajectories and do not appear to be different from those in the region where the literature suggests that adaptation is restricted to (Figure S6). By switching to a robust and efficient sampling method, we have gained a deeper understanding of the quantities of interest in this model. Since these parameter combinations are related to enzymes and their binding affinity, which is highly relevant for drug development (Vellard, 2003; Srinivasan, 2023), effective mathematical modelling of these networks can offer medical insight and support.

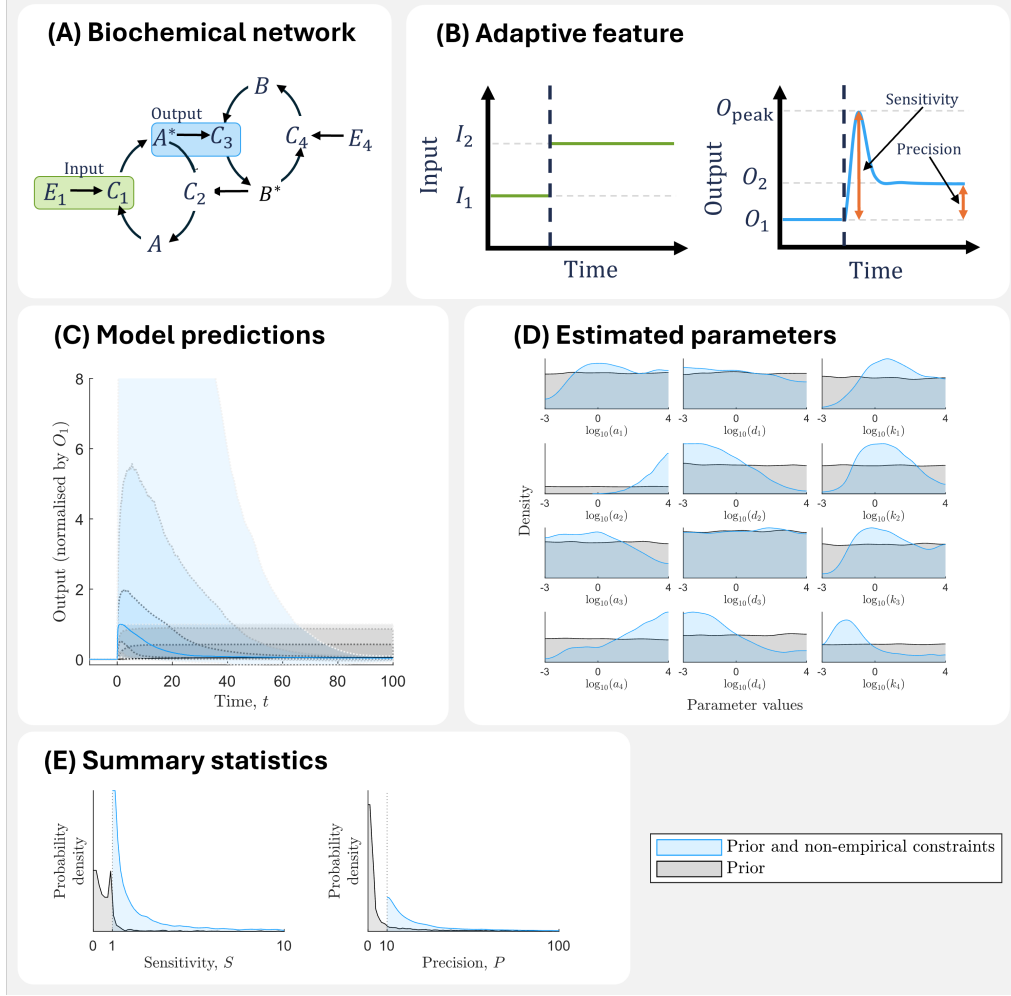


Figure 6: **(A)** A conceptual diagram of the biochemical reaction network capable of adaptation. This diagram depicts a system of protein substrates ( $A$  and  $B$ ), their activated forms ( $A^*$  and  $B^*$ ), enzymes ( $E_1$  and  $E_4$ ), and intermediate protein-protein complexes ( $C_1, C_2, C_3$  and  $C_4$ ) each interacting through biochemical reactions as illustrated by arrows. This biochemical network was used to construct the ordinary differential equation model. Note, in this example we are interested in the input  $I = E_1 + C_1$  and the output  $O = A^* + C_3$ . **(B)** Conceptual diagram of biochemical adaptation, showing the two summary statistics: sensitivity and precision. As the levels of input change (from  $I_1$  to  $I_2$ ; left figure), the output is *sensitive* to the change in stimulus, such that it changes from  $O_1$  to a different concentration  $O_{peak}$ . Additionally, the output is capable of *precisely* returning to its pre-stimulated concentration, such that the output stabilises at a concentration  $O_2$  that is similar to the pre-stimulus level  $O_1$ . **(C)** Model predictions from the prior distribution (grey) and the posterior distribution with the adaptive capability (blue). This figure shows the median prediction and a set of credible intervals (50%, 75% and 90%) for the normalised output after the input has been perturbed at the initial time ( $t = 0$ ). **(D)** The estimated marginal distributions of model parameters both from the prior distribution (grey) and for model parameters that lead to sensitive and precise models (blue). This figure shows that there may be certain areas of parameter space that cannot yield a model capable of biochemical adaptation. **(E)** The measured sensitivity and precision of simulations both from the prior distribution (grey) and from the posterior distribution (blue), where model parameters were sufficiently sensitive ( $S > 1$ ) and precise ( $P > 10$ ) to be considered adaptive.



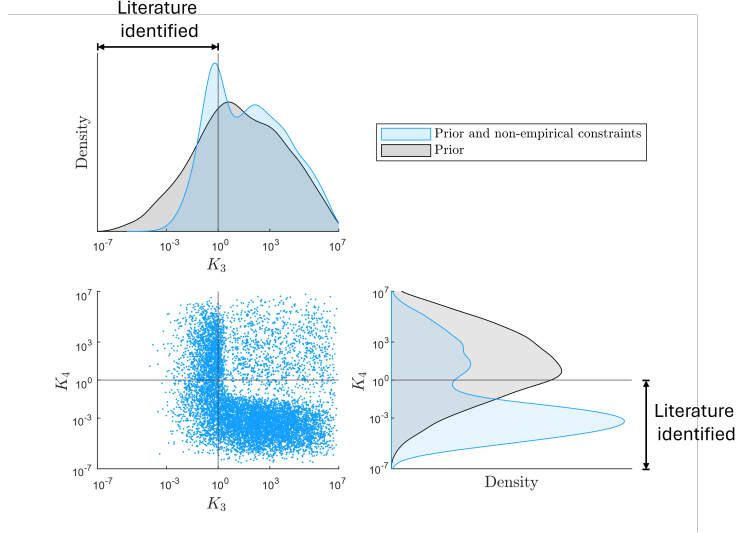


Figure 7: Distributions of the Michaelis-Menten constants  $K_3$  and  $K_4$  from the prior (grey), and the posterior (blue), where the posterior distribution represents models capable of biochemical adaptation, as well as the bivariate distribution from the posterior (blue dots). For comparison, the literature identified  $K_3 < 10^0$  and  $K_4 < 10^0$  as necessary conditions for biochemical adaptation in this network (Jeynes-Smith and Araujo, 2023; Ma et al., 2009).

### 3 Discussion

#### 3.1 Non-empirical information is powerful for calibration

This work presents a general methodology to incorporate any information type – whether empirical or non-empirical – into model calibration. We demonstrate this methodology using three compelling examples from diverse scientific fields that illustrate how integrating non-empirical information can lead to better predictions, inference, management and understanding.

Firstly, using a case study on coral colony recovery, we demonstrated how an expert’s knowledge of typical system function can be used in calibration to remove improbable model dynamics (Figure 1). After calibration, the result is a model that both produces an excellent match to a dataset and aligns with expert beliefs of possible reef recovery dynamics (Figure 3). Given that applied models are often constructed in partnership with the system’s stakeholders (Jakeman et al., 2006; Parrott, 2017), being able to query an expert’s knowledge of the system outputs and easily incorporate these into calibration is a huge asset, especially if done as an iterative process. For example, experts in coral reef recovery dynamics may have specific knowledge of reef recovery dynamics for highly damaged reefs (Warne et al., 2024, 2022), different types of disturbances (Graham et al., 2011), or for specific reef locations (Graham et al., 2011). Our results demonstrate that stakeholder knowledge can transform the predictive capabilities of a fitted model to possess drastically improved precision (Figure 1B), whilst simultaneously refining plausible ranges on model parameters (Figure S1).

Secondly, we generated an ensemble of ecosystem population models that match both short-term monitoring data and long-term behaviours that align with ecological theory (Figure 4). We demonstrated that using both information sources (monitoring data as empirical data and ecological theory as non-empirical information) can alter the predicted consequences of ecosystem management (Figure 5). Given the high uncertainty in parameter values of

ecosystem network models (Baker et al., 2019; Vollert et al., 2024), the limited availability of population time-series datasets (Humbert et al., 2009; McDonald-Madden et al., 2010), which otherwise yield unconstrained and uncertain model predictions (Botelho et al., 2025; Novak et al., 2011), ecosystem network models stand to gain a lot from non-traditional data sources. Beyond the expected theoretical properties of ecosystems (coexistence and stability), there are several additional non-empirical information sources that can be used to inform ecosystem population models, including qualitative population responses to conservation (e.g. the observation that removing feral cats can lead to an increase in rabbit populations and consequently a decrease in native vegetation; see Raymond et al. (2011)), checking whether key model outputs are sensible (e.g., removing vegetation should result in herbivores like rabbits going extinct; see Neil et al. (2025)), or constraining other key quantities (e.g., restricting equilibrium or transient populations to reasonable domains; see Vollert et al. (2025)). When constraining model predictions to fit these non-empirical expectations, the resulting model is better tied to reality, making it far more suitable for the conservation decision-making context it informs.

Finally, we calibrated a model of a biochemical network to exhibit the observed phenomenon of biochemical adaptation (Figure 6). In doing so, we were able to test and challenge conditions stated in the literature that are believed to be required for a biochemical network to express adaptation (Figure 7). In future work, our approach could also be extended to explore and understand many other medically relevant features of homeostasis. For example, the discrepancy function used in our calibration method can include the sensitivity and precision to multiple stimuli to identify parameter sets capable of adaptation for a large range of inputs (see, e.g. Jeynes-Smith and Araujo (2023)); we can explore imperfect adaptation by reducing the requirement on precision tolerance (see, e.g. Bhattacharya et al. (2023)); the time to adaptation can be incorporated to ensure that adaptation occurs in a biologically meaningful time-frame; and the model can be made stochastic to account for the randomness inherent in biochemical systems (Briat et al., 2016). Prior to our study, it was not possible for these important concepts to be thoroughly explored via simulation due to computational limitations. Using our efficient and rigorous search algorithm, we generated a larger sample of parameter sets capable of biochemical adaptation than previous literature; e.g., Ma et al. (2009) and Jeynes-Smith and Araujo (2023) test  $10^5$  parameter sets, with  $\sim 1\%$  of these producing adaptation, whereas we have obtained  $10^5$  parameter sets all of which are capable of adaptation.

Across all three demonstrated examples, non-empirical data — field knowledge of possible versus impossible system properties, theoretical long-term behaviour, and frequently observed phenomena — were used to refine the plausible parameter space of simulation models, providing more realistic predictions (Figures 1, 3, 4 and 6) and more informed inferences (Figures S1, S3, S4 and 6). For each case study, the results and findings are substantial for that field, yet we have only scratched the surface of what these methods could achieve.

### 3.2 Opportunities are unlocked by rigorous and systematic statistics

The approach that we propose has three distinct methodological benefits: it provides a framework for calibration with a likelihood and approximate likelihood function simultaneously, it robustly and efficiently samples this distribution via our new SMC sampler, and it can be used as a novel simulation-based prior elicitation method.

The literature for parameterising models using data is extensive (Sisson et al., 2018; McElreath, 2018; Martin et al., 2024), but very few studies have looked at non-empirical constraints (Barnes et al., 2011; Vollert et al., 2025). To the authors’ knowledge, this is the

first formal calibration framework for both data and non-empirical features simultaneously. Here, we have defined a distribution that combines a likelihood with a discrepancy function (Equation (14)), allowing any information to be easily encoded into parameterisation via specification of these functions (see Methods section 4.3). This novel combination of data sources allows models to leverage the specificity of data, as well as the broad effects of non-empirical constraints. For example, in Section 2.2, [Case study 2: Ecosystem population modelling](#), we showed that population time-series datasets honed in on the magnitude of species populations (Figure 4B), whilst the constraints on long-term population dynamics ensured that the system as a whole functioned according to ecological theory (Figure 4C). While some models have been previously parameterised with a combination of data and non-empirical sources, these sampling algorithms have been ad-hoc, inefficient and not easily generalisable to new information (see e.g., typical processes in ecological network modelling (Neil et al., 2025; Peterson et al., 2021; Baker et al., 2019) that rely on rejection sampling and optimisation algorithms). However, as a direct consequence of formalising the target distribution for calibration to non-empirical information (Equation (14)), established sampling regimes can be leveraged. We developed an efficient and robust SMC algorithm that simultaneously anneals the likelihood and discrepancy (see Supplementary Material Section S.3).

Additionally, our statistical framework addresses a key challenge in Bayesian model calibration: defining the prior distribution (Banner et al., 2020). Since many model parameters lack physical meaning or cannot be measured (e.g., consider the species interaction strengths in Section 2.2, [Case study 2: Ecosystem population modelling](#)), developing methods for specifying prior distributions is an open challenge (Mikkola et al., 2024). Our method can be considered a novel approach to prior elicitation because it uses prior knowledge of reasonable outputs to infer an informed prior distribution via simulation. For example, in Section 2.1, [Case study 1: Logistic coral growth](#), we infer the informed prior distribution that yields plausible coral reef recovery dynamics according to prior knowledge of coral reef recovery times (Figure S1), and this informed prior can be simultaneously included in Bayesian inference with data (Figure S3).

When considered as a prior elicitation method, our approach has three key advantages. First, our method systematically includes prior predictive checks within our inference process, as all coral reef recovery predictions from the informed prior distribution must satisfy the expert’s prior knowledge of recovery dynamics (Figure 1). Second, in comparison to other prior elicitation methods, our approach is highly flexible and generalisable since it does not require manual specification of prior distributions to test (see e.g., Wesner and Pomeranz (2021)), or hyperparameters of the prior distribution (see e.g., Bockting et al. (2024)) and, therefore, does not rely on specifying a parametric family for the prior. Third, our prior elicitation method automatically captures the parameter interdependency structure via simulation, which is an otherwise ongoing challenge in prior elicitation (Mikkola et al., 2024), and resolving this problem is particularly important when constraints do not have a straightforward effect on individual parameter values (Figure 2). Hence, this new method represents a novel and generalisable simulation-based method for eliciting the joint prior distribution including its dependency structure.

### 3.3 Building trust via model calibration in high uncertainty

Whilst our methodology treats information for model calibration as generally irrefutable, we recognise that elicited knowledge can contain uncertainties and biases (O’Hagan, 2019), which may need to be treated with uncertainty (Krueger et al., 2012), much like a likelihood function treats data with uncertainty. As such, confidence needs to be attributed to any non-empirical information, and practitioners should consider using conservative estimates,

following elicitation guidelines (Hemming et al., 2018), and testing parameter sensitivity to non-empirical features (Saltelli et al., 2006). When the alternative is no data or limited data, it is our view that uncertain expert-elicited knowledge is still valuable and should not be ignored in model calibration. After all, empirical data can also be highly uncertain and biased, sparking concerns of trust in models built on such data (Harper et al., 2021; Vilas et al., 2023). However, through connecting to additional and varied sources of information, our approach may help to alleviate such concerns, e.g., by eliminating implausible model predictions (Case study 1: Logistic coral growth), incorporating theory-based expectations (Case study 2: Ecosystem population modelling), and broadening the parameter space when identifying models that recover observed system behaviours (Case study 3: Biochemical adaptation).

In this work, we have shown how non-empirical information can be mathematically utilised to provide a critically valuable resource for model calibration. Ultimately, leveraging the vast knowledge bases found in well-studied systems could be the key to better management and a better understanding of systems across science.

## 4 Methods

### 4.1 Bayesian model calibration

Model calibration (parameter estimation) is the process by which the parameters of a mathematical model are adjusted to align its outputs with the underlying observed system. Consider a model  $M(\theta)$ , where  $\theta$  is the set of model parameters. The goal of model calibration is to infer the parameters  $\theta$ , such that the outputs of the model  $M(\theta)$  are consistent with the data observed  $\mathbf{y}_{\text{obs}}$ . In Bayesian model calibration we aim to obtain a probability distribution of values  $\theta$  according to both the likelihood of the data arising from parameter values and the prior probability of parameter values. Bayesian inference provides a coherent statistical framework for combining this information to form a posterior distribution (McElreath, 2018; Girolami, 2008; Martin et al., 2024):

$$\pi(\theta|\mathbf{y}_{\text{obs}}) \propto \pi(\theta)f(\mathbf{y}_{\text{obs}}|\theta). \quad (12)$$

Here,  $\pi(\theta)$  is the prior distribution, representing our initial belief about the parameters  $\theta$  before observing any data, and  $f(\mathbf{y}_{\text{obs}}|\theta)$  is the likelihood function, representing the probability of the observed data  $\mathbf{y}_{\text{obs}}$  given the parameters  $\theta$  when generated using the model  $M(\theta)$ . The posterior distribution  $\pi(\theta|\mathbf{y}_{\text{obs}})$  combines the prior information with the data to yield a representation of the probability of model parameter values  $\theta$  for the given observed data  $\mathbf{y}_{\text{obs}}$ .

Bayesian model calibration is a foundational tool for finding an appropriate distribution of parameter values that match mathematical models to the data. Using a sampling algorithm – such as Markov chain Monte Carlo (MCMC; Gamerman and Lopes, 2006) or sequential Monte Carlo (SMC; Del Moral et al., 2006; Chopin, 2002) – an ensemble of parameter samples from the posterior distribution can be obtained and fed into these models for predictions that aim to match real-world observations. However, it remains a challenge to understand how non-empirical data fits within this framework because the likelihood function cannot be easily defined.

## 4.2 Approximate Bayesian inference

Approximate Bayesian computation (ABC) is a model calibration framework used when the likelihood cannot be calculated. These methods approximate the likelihood function by comparing model simulations to observations and measuring the discrepancy between them (Beaumont, 2019; Sisson et al., 2018; Sunnåker et al., 2013; Beaumont, 2010). Here, we consider ABC methods because the likelihood may not be calculable when the data source is non-empirical, such as expert judgment or qualitative insights. For example, it would be challenging to define the likelihood function for an ecologist’s observation that ecosystem populations must have a stable equilibrium (see Section 2.2, Case study 2: Ecosystem population modelling).

Approximate Bayesian frameworks compare simulated data  $\mathbf{y}_{\text{sim}}(\boldsymbol{\theta})$  for the model specified by  $\boldsymbol{\theta}$ , to the observed data  $\mathbf{y}_{\text{obs}}$  using two key functions: a summarisation function, and a discrepancy function. The summarisation function  $S(\cdot)$  reduces the information from the full dataset  $\mathbf{y}_{\text{obs}}$  or model simulation  $\mathbf{y}_{\text{sim}}(\boldsymbol{\theta})$  to a small set of comparable summary statistics  $\mathbf{S}_{\text{obs}} = S(\mathbf{y}_{\text{obs}})$  and  $\mathbf{S}_{\text{sim}}(\boldsymbol{\theta}) = S(\mathbf{y}_{\text{sim}}(\boldsymbol{\theta}))$  which retain the key information needed to compare  $\mathbf{y}_{\text{obs}}$  to  $\mathbf{y}_{\text{sim}}(\boldsymbol{\theta})$ ; e.g., the mean and variance are common summary statistics. A discrepancy function  $\rho(\cdot)$  is then used to characterise the difference between the summary statistics for the observed data  $\mathbf{S}_{\text{obs}}$  and the simulated data  $\mathbf{S}_{\text{sim}}(\boldsymbol{\theta})$ . As such, the discrepancy  $\rho \equiv \rho(\mathbf{S}_{\text{obs}}, \mathbf{S}_{\text{sim}}(\boldsymbol{\theta}))$  can be used to assess whether the parameter values are plausible based on how closely the summary statistics match. This discrepancy function is non-negative and produces a scalar discrepancy score  $\rho$  that is 0 if  $\mathbf{S}_{\text{obs}} = \mathbf{S}_{\text{sim}}(\boldsymbol{\theta})$  and  $> 0$  when  $\mathbf{S}_{\text{obs}} \neq \mathbf{S}_{\text{sim}}(\boldsymbol{\theta})$ .

In ABC, a parameter set  $\boldsymbol{\theta}$  is typically accepted as plausible if the discrepancy  $\rho$  between simulated and observed summaries is below some threshold  $\epsilon$ . Therefore, the discrepancy function can be used to approximate the likelihood, as both the discrepancy and likelihood assess the ability of the parameters to produce the observed outputs:

$$f(\mathbf{y}_{\text{obs}}|\boldsymbol{\theta}) \approx \int \mathbb{I}(\rho(S(\mathbf{y}_{\text{sim}}(\boldsymbol{\theta})), S(\mathbf{y}_{\text{obs}})) < \epsilon | \boldsymbol{\theta}) d\mathbf{y}_{\text{sim}},$$

where  $\mathbb{I}(\cdot)$  is an indicator function that is 1 when the condition inside is true, and 0 otherwise. Using this approximation of the likelihood, the posterior distribution  $\pi(\boldsymbol{\theta}|\mathbf{y}_{\text{obs}})$  can be approximated as  $\pi_{\epsilon}(\boldsymbol{\theta}|\mathbf{y}_{\text{obs}})$  given by

$$\pi_{\epsilon}(\boldsymbol{\theta}|\mathbf{y}_{\text{obs}}) \propto \pi(\boldsymbol{\theta}) \int \mathbb{I}(\rho(S(\mathbf{y}_{\text{sim}}(\boldsymbol{\theta})), S(\mathbf{y}_{\text{obs}})) < \epsilon | \boldsymbol{\theta}) d\mathbf{y}_{\text{sim}}.$$

Parameter values from the approximate posterior  $\pi_{\epsilon}(\boldsymbol{\theta}|\mathbf{y}_{\text{obs}})$  can be sampled using a variety of methods, such as ABC-MCMC (Marjoram et al., 2003) or ABC-SMC (Del Moral et al., 2012); see Sisson et al. (2018) or Beaumont (2019) for an overview.

## 4.3 Incorporating non-empirical data in Bayesian inference

Traditionally, ABC converts empirical data to carefully chosen summary statistics for comparison. However, if the summarised features of the data can be obtained directly – for example, via expert elicitation, observation, logic, physical rules, or even hypothesis – these could also be used for model calibration. In traditional ABC, summary statistics are calculated from empirical data as  $\mathbf{S}_{\text{obs}} = S(\mathbf{y}_{\text{obs}})$ , here we relax this requirement such that non-empirical data sources are treated as directly observed summary statistics  $\mathbf{S}_{\text{obs}}$ . For example, an ecologist’s observation that coral populations can recover to carrying capacity within 50 years can be used as a summary statistic even if there is no empirical data available to estimate this statistic (see Section 2.1, Case study 1: Logistic coral growth). In our

non-empirical framework, the summary statistics are constructed based on (a) what information  $\mathbf{S}_{\text{obs}}$  can be known with confidence, and (b) whether this summary statistic can be measured from model outputs  $\mathbf{S}_{\text{sim}} = \mathbf{S}(\mathbf{y}_{\text{sim}})$ . For example, an ecologist must be confident that coral cover cannot exceed 10% within 5 years post-disturbance, and the model must be able to simulate coral cover through time (see Section 2.1, [Case study 1: Logistic coral growth](#)).

Compared to summary statistics calculated from empirical data, we often cannot elicit an exact value of a summary statistic from non-empirical sources. Continuing with our coral cover example, if data were routinely collected at various reefs 5 years after a disturbance, then the mean coral cover 5 years post-disturbance could be calculated from the empirical dataset. However, in the absence of this empirical data, it is a challenge for an ecologist to estimate the mean coral cover with confidence, and it is far easier to elicit a range of values for the summary statistic, such that coral cover should be less than 10%.

Whether the summary statistic is an exact value (calculated from an empirical dataset,  $S_{\text{obs}} = S(\mathbf{y}_{\text{obs}}) = a$ ) or a range of values (elicited from experts,  $S_{\text{obs}} \leq a$ ) is an artefact of the available data for model calibration, yet having a range of values for a summary statistic is a relatively strange concept in ABC that requires subtle changes to the statistical formulation (see Table 2). A traditional ABC discrepancy function  $\rho(\cdot)$  would describe the distance between the observed and simulated summary statistic, and this discrepancy score would be minimised to some tolerance  $\epsilon$  to approximate the likelihood. Instead, where the observed summary statistic is expressed as a range, the discrepancy must measure the distance to the acceptable range (achieved using minimisation or maximisation functions) and we aim to find parameter sets that lead to no discrepancy  $\epsilon = 0$ . In the coral growth example, this discrepancy would measure how far above 10% the coral cover is after 5 years, and we would only accept models with no discrepancy, i.e., no predictions over 10%. These subtle differences from empirical ABC (summarised in Table 2) shift the calibration towards rejecting models with impossible outputs, rather than closely matching empirical datasets.

	<b>Empirical ABC</b>	<b>Non-empirical ABC</b>
Observed summary statistic	$S_{\text{obs}} = S(\mathbf{y}_{\text{obs}}) = a$	$S_{\text{obs}} \leq a$
Simulated summary statistic	$S_{\text{sim}}(\boldsymbol{\theta}) = S(\mathbf{y}_{\text{sim}}(\boldsymbol{\theta})) = b$	$S_{\text{sim}}(\boldsymbol{\theta}) = S(\mathbf{y}_{\text{sim}}(\boldsymbol{\theta})) = b$
Discrepancy function	$\rho(S_{\text{obs}}, S_{\text{sim}}) =  b - a $	$\rho(S_{\text{obs}}, S_{\text{sim}}) = \max(b - a, 0)$
Likelihood approximation	$\mathbb{I}(\rho(S_{\text{obs}}, S_{\text{sim}}) < \epsilon)$	$\mathbb{I}(\rho(S_{\text{obs}}, S_{\text{sim}}) = 0)$

Table 2: An example of the potential differences between empirical and non-empirical ABC.

For a given set of non-empirical data  $\mathbf{S}_{\text{obs}}$  and their corresponding summary statistics and discrepancy function (e.g., as in Table 2), an approximate posterior can be defined as

$$\pi(\boldsymbol{\theta} | \mathbf{S}_{\text{obs}}) \propto \pi(\boldsymbol{\theta}) \int \mathbb{I}(\rho(\mathbf{S}_{\text{obs}}, S(\mathbf{y}_{\text{sim}}(\boldsymbol{\theta}))) = 0 | \boldsymbol{\theta}) d\mathbf{y}_{\text{sim}},$$

and parameter sets sampled using any ABC sampling approach.

Additionally, non-empirical data can be combined with empirical data; via a likelihood function, such as a Gaussian likelihood,

$$f(\mathbf{y}_{\text{obs}} | \boldsymbol{\theta}) = \prod_{i=1}^n f(y_{\text{obs},i} | \boldsymbol{\theta}) = \prod_{i=1}^n \frac{1}{\sqrt{2\pi}\sigma} \exp\left(-\frac{y_{\text{sim},i}(\boldsymbol{\theta}) - y_{\text{obs},i}}{2\sigma^2}\right) \quad (13)$$

where  $f(\mathbf{y}_{\text{obs}} | \boldsymbol{\theta})$  is the likelihood of observing data  $\mathbf{y}_{\text{obs}}$  from a model characterised by parameters  $\boldsymbol{\theta}$ ,  $n$  is the number of observed data points,  $y_{\text{obs},i}$  is the  $i$ th observation,  $\sigma$  is a parameter representing measurement noise, and  $y_{\text{sim},i}$  is the data simulated by the model

characterised by parameters  $\theta$  with equivalent inputs to that of data point  $i$ . Using a likelihood to describe the probability that the model defined by a set of parameters  $\theta$  produced the dataset  $\mathbf{y}_{\text{obs}}$ , we can target both the non-empirical observations and the traditional Bayesian posterior (as in Equation (12));

$$\pi(\theta|S_{\text{obs}}, \mathbf{y}_{\text{obs}}) \propto \pi(\theta)f(\mathbf{y}_{\text{obs}}|\theta) \int \mathbb{I}\left(\rho(S_{\text{obs}}, S(\mathbf{y}_{\text{sim}}(\theta))) = 0 \middle| \theta\right) d\mathbf{y}_{\text{sim}}. \quad (14)$$

This combination of empirical and non-empirical data means highly data-limited scenarios can still take advantage of any available information.

Sampling this distribution can be done by leveraging existing methods of sampling an exact or approximate distribution. In this work, we have developed a novel modification of the SMC-ABC algorithm proposed by [Drovandi and Pettitt \(2011\)](#), to efficiently sample the distribution in Equation (14). This algorithm sequentially reduces the discrepancy and anneals the likelihood by iteratively reweighting, resampling and moving an ensemble of parameter sets until a posterior distribution with no discrepancy is obtained (see Supplementary Material S.3 for details). This adaptive and simultaneous incorporation of both the likelihood and approximate likelihood allows for flexible, efficient and robust sampling of the distribution which both matches the data and the non-empirical constraints.

## Data and code availability

All data needed to evaluate the conclusions in the paper are present in the paper and/or the Supplementary Materials. MATLAB code used to generate the results in this paper is available in the Figshare Repository: <https://doi.org/10.6084/m9.figshare.29115044>. Code to use the methods developed in this paper is available in R (<https://github.com/luzvpascal/SMCfeatures>) and in MATLAB (<https://doi.org/10.6084/m9.figshare.29115044>).

## Acknowledgements

SAV is supported by a Queensland University of Technology Centre for Data Science, Australia Scholarship and a Statistical Society of Australia Top-Up Scholarship. CD and LVP are supported by an Australian Research Council Discovery Project (DP200102101). LVP acknowledges funding from an Australian Research Council Discovery Early Career Researcher Award (DE200101791). MPA and SAV acknowledge funding support from an Australian Research Council Discovery Early Career Researcher Award (DE200100683). LVP and MPA acknowledge funding from the ARC SRIEAS Grant SR200100005 Securing Antarctica's Environmental Future. The eResearch Office, Queensland University of Technology provided computational resources.



## References

- Adams, M. P., S. A. Sisson, K. J. Helmstedt, C. M. Baker, M. H. Holden, M. Plein, J. Holloway, K. L. Mengersen, and E. McDonald-Madden (2020). Informing management decisions for ecological networks, using dynamic models calibrated to noisy time-series data. *Ecology Letters* 23(4), 607–619. 9, 10, 11
- Allesina, S. and S. Tang (2012). Stability criteria for complex ecosystems. *Nature* 483(7388), 205–208. 9, 10, 33
- Aoki, S. K., G. Lillacci, A. Gupta, A. Baumschlager, D. Schweingruber, and M. Khammash (2019). A universal biomolecular integral feedback controller for robust perfect adaptation. *Nature* 570(7762), 533–537. 13
- Araujo, R. P. and L. A. Liotta (2018). The topological requirements for robust perfect adaptation in networks of any size. *Nature Communications* 9(1), 1757. 13
- Araujo, R. P. and L. A. Liotta (2023). Only a topological method can identify all possible network structures capable of robust perfect adaptation. *PLoS Computational Biology* 19(11), e1011638. 13
- Assumpção, T. H., I. Popescu, A. Jonoski, and D. P. Solomatine (2018). Citizen observations contributing to flood modelling: Opportunities and challenges. *Hydrology and Earth System Sciences* 22(2), 1473–1489. 2, 4
- Aster, R. C., B. Borchers, and C. H. Thurber (2018). *Parameter estimation and inverse problems*. Elsevier. 2
- Australian Institute of Marine Science (2015). Long-term Monitoring Program: Crown-of-thorns starfish and benthos Manta Tow Data (Great Barrier Reef). <https://doi.org/10.25845/5c09b0abf315a> [Accessed: 23-01-2025]. 8
- Australian Institute of Marine Science (2024). Long-Term Monitoring Program. <https://www.aims.gov.au/research-topics/monitoring-and-discovery/monitoring-great-barrier-reef/long-term-monitoring-program> [Accessed: 23-01-2025]. 5, 8
- Baker, C. M., M. Bode, N. Dexter, D. B. Lindenmayer, C. Foster, C. MacGregor, M. Plein, and E. McDonald-Madden (2019). A novel approach to assessing the ecosystem-wide impacts of reintroductions. *Ecological Applications* 29(1), e01811. 9, 10, 17, 18
- Baker, C. M., A. Gordon, and M. Bode (2017). Ensemble ecosystem modeling for predicting ecosystem response to predator reintroduction. *Conservation Biology* 31(2), 376–384. 9, 10
- Banner, K. M., K. M. Irvine, and T. J. Rodhouse (2020). The use of Bayesian priors in ecology: The good, the bad and the not great. *Methods in Ecology and Evolution* 11, 882–889. 3, 18
- Barnes, C. P., D. Silk, X. Sheng, and M. P. Stumpf (2011). Bayesian design of synthetic biological systems. *Proceedings of the National Academy of Sciences* 108(37), 15190–15195. 3, 17
- Beaumont, M. A. (2010). Approximate Bayesian computation in evolution and ecology. *Annual review of ecology, evolution, and systematics* 41, 379–406. 20
- Beaumont, M. A. (2019). Approximate Bayesian computation. *Annual review of statistics and its application* 6, 379–403. 3, 20, 40

- Bellomo, N., G. A. Marsan, and A. Tosin (2013). *Complex systems and society: modeling and simulation*, Volume 2. Springer. [2](#)
- Bhagowati, B. and K. U. Ahamad (2019). A review on lake eutrophication dynamics and recent developments in lake modeling. *Ecohydrology & Hydrobiology* 19(1), 155–166. [4](#)
- Bhattacharya, P., K. Raman, and A. K. Tangirala (2023). On biological networks capable of robust adaptation in the presence of uncertainties: A linear systems-theoretic approach. *Mathematical Biosciences* 358, 108984. [17](#)
- Bockting, F., S. T. Radev, and P.-C. Bürkner (2024). Simulation-based prior knowledge elicitation for parametric Bayesian models. *Scientific Reports* 14(1), 17330. [18](#)
- Bode, M., C. M. Baker, J. Benshemesh, T. Burnard, L. Rumpff, C. E. Hauser, J. J. Lahoz-Monfort, and B. A. Wintle (2017). Revealing beliefs: using ensemble ecosystem modelling to extrapolate expert beliefs to novel ecological scenarios. *Methods in Ecology and Evolution* 8(8), 1012–1021. [10](#)
- Botelho, L. L., C. Jeynes-Smith, S. Vollert, and M. Bode (2025). Ecosystem models cannot predict the consequences of conservation decisions. *Ecology Letters* 28(1), e70034. [2](#), [10](#), [17](#)
- Briat, C., A. Gupta, and M. Khammash (2016). Antithetic integral feedback ensures robust perfect adaptation in noisy biomolecular networks. *Cell Systems* 2(1), 15–26. [13](#), [17](#)
- Britton, T. and G. Scalia Tomba (2019). Estimation in emerging epidemics: biases and remedies. *Journal of the Royal Society Interface* 16(150), 20180670. [2](#)
- Carpenter, S. R., D. Ludwig, and W. A. Brock (1999). Management of eutrophication for lakes subject to potentially irreversible change. *Ecological Applications* 9(3), 751–771. [4](#)
- Chopin, N. (2002). A sequential particle filter method for static models. *Biometrika* 89(3), 539–552. [3](#), [19](#), [40](#)
- Confavreux, C., S. Vukusic, T. Moreau, and P. Adeleine (2000). Relapses and progression of disability in multiple sclerosis. *New England Journal of Medicine* 343(20), 1430–1438. [4](#)
- Craver, C. F. (2006). When mechanistic models explain. *Synthese* 153(3), 355–376. [2](#)
- Cuddington, K. (2001). The “balance of nature” metaphor and equilibrium in population ecology. *Biology and Philosophy* 16, 463–479. [9](#)
- Cuffey, K. M. and E. J. Brook (2000). Ice sheets and the ice-core record of climate change. In *International Geophysics*, Volume 72, pp. 459–497. Elsevier. [4](#)
- Del Moral, P., A. Doucet, and A. Jasra (2006). Sequential Monte Carlo samplers. *Journal of the Royal Statistical Society: Series B (Statistical Methodology)* 68(3), 411–436. [3](#), [19](#), [40](#)
- Del Moral, P., A. Doucet, and A. Jasra (2012). An adaptive sequential Monte Carlo method for approximate Bayesian computation. *Statistics and Computing* 22(5), 1009–1020. [7](#), [20](#)
- Deligne, N. I., G. E. Jolly, T. Taig, and T. H. Webb (2018). Evaluating life-safety risk for fieldwork on active volcanoes: the volcano life risk estimator (VoLREst), a volcano observatory’s decision-support tool. *Journal of Applied Volcanology* 7(1), 1–19. [2](#)
- Dommenget, D. and J. Flöter (2011). Conceptual understanding of climate change with a globally resolved energy balance model. *Climate Dynamics* 37, 2143–2165. [4](#)

- Dougoud, M., L. Vinckenbosch, R. P. Rohr, L.-F. Bersier, and C. Mazza (2018). The feasibility of equilibria in large ecosystems: A primary but neglected concept in the complexity-stability debate. *PLoS Computational Biology* 14(2), e1005988. [9](#)
- Drovandi, C. C. and A. N. Pettitt (2011). Estimation of parameters for macroparasite population evolution using approximate Bayesian computation. *Biometrics* 67(1), 225–233. [3](#), [7](#), [22](#), [35](#), [41](#)
- Fava, M. C., N. Abe, C. Restrepo-Estrada, B. Y. Kimura, and E. M. Mendiondo (2019). Flood modelling using synthesised citizen science urban streamflow observations. *Journal of Flood Risk Management* 12(S2), e12498. [4](#)
- Felce, D. and J. Perry (1995). Quality of life: Its definition and measurement. *Research in Developmental Disabilities* 16(1), 51–74. [2](#)
- Ferrell, J. E. (2016). Perfect and near-perfect adaptation in cell signaling. *Cell Systems* 2(2), 62–67. [13](#)
- Friston, K. J., T. Parr, P. Zeidman, A. Razi, G. Flandin, J. Daunizeau, O. J. Hulme, A. J. Billig, V. Litvak, C. J. Price, et al. (2020). Effective immunity and second waves: a dynamic causal modelling study. *Wellcome Open Research* 5, 204. [4](#)
- Gamerman, D. and H. F. Lopes (2006). *Markov chain Monte Carlo: Stochastic simulation for Bayesian inference*. CRC Press. [19](#), [40](#)
- Geary, W. L., M. Bode, T. S. Doherty, E. A. Fulton, D. G. Nimmo, A. I. Tulloch, V. J. Tulloch, and E. G. Ritchie (2020). A guide to ecosystem models and their environmental applications. *Nature Ecology & Evolution* 4(11), 1459–1471. [2](#)
- Gelman, A., D. Simpson, and M. Betancourt (2017). The prior can often only be understood in the context of the likelihood. *Entropy* 19(10), 555. [3](#)
- Girolami, M. (2008). Bayesian inference for differential equations. *Theoretical Computer Science* 408, 4 – 16. [19](#)
- Graham, N., K. Nash, and J. Kool (2011). Coral reef recovery dynamics in a changing world. *Coral Reefs* 30, 283–294. [16](#)
- Grilli, J., M. Adorisio, S. Suweis, G. Barabás, J. R. Banavar, S. Allesina, and A. Maritan (2017). Feasibility and coexistence of large ecological communities. *Nature Communications* 8(1), 1–8. [9](#), [10](#), [32](#)
- Harper, A., N. Mustafee, and M. Yearworth (2021). Facets of trust in simulation studies. *European Journal of Operational Research* 289(1), 197–213. [2](#), [19](#)
- Hemming, V., M. A. Burgman, A. M. Hanea, M. F. McBride, and B. C. Wintle (2018). A practical guide to structured expert elicitation using the IDEA protocol. *Methods in Ecology and Evolution* 9(1), 169–180. [19](#)
- Holme, P. and F. Liljeros (2015). Mechanistic models in computational social science. *Frontiers in Physics* 3, 78. [2](#)
- Humbert, J.-Y., L. Scott Mills, J. S. Horne, and B. Dennis (2009). A better way to estimate population trends. *Oikos* 118(12), 1940–1946. [17](#)
- Jakeman, A. J., R. A. Letcher, and J. P. Norton (2006). Ten iterative steps in development and evaluation of environmental models. *Environmental Modelling & Software* 21(5), 602–614. [16](#)

- Jasra, A., D. A. Stephens, A. Doucet, and T. Tsagaris (2011). Inference for lévy-driven stochastic volatility models via adaptive sequential Monte Carlo. *Scandinavian Journal of Statistics* 38(1), 1–22. [41](#)
- Jeremiah, E., S. A. Sisson, A. Sharma, and L. Marshall (2012). Efficient hydrological model parameter optimization with Sequential Monte Carlo sampling. *Environmental Modelling & Software* 38, 283–295. [40](#)
- Jeynes-Smith, C. and R. Araujo (2023). Protein–protein complexes can undermine ultrasensitivity-dependent biological adaptation. *Journal of the Royal Society Interface* 20(198), 20220553. [13](#), [14](#), [16](#), [17](#), [34](#), [35](#)
- Karl, T. R., J. D. Tarpley, R. G. Quayle, H. F. Diaz, D. A. Robinson, and R. S. Bradley (1989). The recent climate record: What it can and cannot tell us. *Reviews of Geophysics* 27(3), 405–430. [2](#)
- Karp, R. L., M. P. Millán, T. Dasgupta, A. Dickenstein, and J. Gunawardena (2012). Complex-linear invariants of biochemical networks. *Journal of Theoretical Biology* 311, 130–138. [13](#)
- Khammash, M. H. (2021). Perfect adaptation in biology. *Cell Systems* 12(6), 509–521. [13](#)
- Kitano, H. (2002). Computational systems biology. *Nature* 420(6912), 206–210. [2](#)
- Krueger, T., T. Page, K. Hubacek, L. Smith, and K. Hiscock (2012). The role of expert opinion in environmental modelling. *Environmental Modelling & Software* 36, 4–18. [3](#), [18](#)
- Landi, P., H. O. Minoarivelo, Å. Brännström, C. Hui, and U. Dieckmann (2018). Complexity and stability of adaptive ecological networks: a survey of the theory in community ecology. In *Systems analysis approach for complex global challenges*, pp. 209–248. Springer. [9](#)
- Levin, L. A., B. J. Bett, A. R. Gates, P. Heimbach, B. M. Howe, F. Janssen, A. McCurdy, H. A. Ruhl, P. Snelgrove, K. I. Stocks, et al. (2019). Global observing needs in the deep ocean. *Frontiers in Marine Science* 6, 241. [2](#)
- Lundby, C. and P. Robach (2015). Performance enhancement: what are the physiological limits? *Physiology*. [4](#)
- Ma, W., A. Trusina, H. El-Samad, W. A. Lim, and C. Tang (2009). Defining network topologies that can achieve biochemical adaptation. *Cell* 138(4), 760–773. [13](#), [14](#), [16](#), [17](#), [35](#)
- Malone, H., J. Yang, D. L. Hershman, J. D. Wright, J. N. Bruce, and A. I. Neugut (2015). Complications following stereotactic needle biopsy of intracranial tumors. *World Neurosurgery* 84(4), 1084–1089. [2](#)
- Marjoram, P., J. Molitor, V. Plagnol, and S. Tavaré (2003). Markov chain Monte Carlo without likelihoods. *Proceedings of the National Academy of Sciences* 100(26), 15324–15328. [20](#)
- Martin, G. M., D. T. Frazier, and C. P. Robert (2024). Computing Bayes: From then ‘til now. *Statistical Science* 39(1), 3–19. [2](#), [17](#), [19](#), [40](#)
- McDonald-Madden, E., P. W. Baxter, R. A. Fuller, T. G. Martin, E. T. Game, J. Montambault, and H. P. Possingham (2010). Monitoring does not always count. *Trends in Ecology & Evolution* 25(10), 547–550. [17](#)
- McElreath, R. (2018). *Statistical rethinking: A Bayesian course with examples in R and Stan*. Chapman and Hall/CRC. [2](#), [17](#), [19](#)

- Mikkola, P., O. A. Martin, S. Chandramouli, M. Hartmann, O. Abril Pla, O. Thomas, H. Pesonen, J. Corander, A. Vehtari, S. Kaski, et al. (2024). Prior knowledge elicitation: The past, present, and future. *Bayesian Analysis* 19(4), 1129–1161. [3](#), [18](#)
- Monsalve-Bravo, G. M., B. A. J. Lawson, C. Drovandi, K. Burrage, K. S. Brown, C. M. Baker, S. A. Vollert, K. Mengersen, E. McDonald-Madden, and M. P. Adams (2022). Analysis of sloppiness in model simulations: Unveiling parameter uncertainty when mathematical models are fitted to data. *Science Advances* 8(38), eabm5952. [10](#)
- Mouquet, N., Y. Lagadeuc, V. Devictor, L. Doyen, A. Duputié, D. Eveillard, D. Faure, E. Garnier, O. Gimenez, P. Huneman, et al. (2015). Predictive ecology in a changing world. *Journal of Applied Ecology* 52(5), 1293–1310. [2](#)
- Murray, J. D. (2002). *Mathematical Biology I: An Introduction*. Springer, New York, New York, USA. [4](#)
- Neil, E., E. Carrella, and R. Bailey (2025). Calibrating multi-constraint ensemble ecosystem models using genetic algorithms and Approximate Bayesian Computation: A case study of rewilding at the Knepp Estate, UK. *Ecological Modelling* 500, 110948. [17](#), [18](#)
- Novak, M., J. T. Wootton, D. F. Doak, M. Emmerson, J. A. Estes, and M. T. Tinker (2011). Predicting community responses to perturbations in the face of imperfect knowledge and network complexity. *Ecology* 92(4), 836–846. [17](#)
- O’Hagan, A. (2019). Expert knowledge elicitation: subjective but scientific. *The American Statistician* 73, 69–81. [18](#)
- Parrott, L. (2017). The modelling spiral for solving ‘wicked’ environmental problems: Guidance for stakeholder involvement and collaborative model development. *Methods in Ecology and Evolution* 8(8), 1005–1011. [16](#)
- Pascal, L. V., S. A. Vollert, M. D. Bimler, C. M. Baker, M. Vernet, S. Canessa, C. Drovandi, and M. P. Adams (2025). EEMtoolbox: A user-friendly R package for flexible ensemble ecosystem modeling. *Methods in Ecology and Evolution*, 1–9. [10](#)
- Pech, R. and G. Hood (1998). Foxes, rabbits, alternative prey and rabbit calicivirus disease: consequences of a new biological control agent for an outbreaking species in Australia. *Journal of Applied Ecology* 35(3), 434–453. [10](#)
- Pesendorfer, M. B., C. M. Baker, M. Stringer, E. McDonald-Madden, M. Bode, A. K. McEachern, S. A. Morrison, and T. S. Sillett (2018). Oak habitat recovery on California’s largest islands: scenarios for the role of corvid seed dispersal. *Journal of Applied Ecology* 55(3), 1185–1194. [10](#)
- Peterson, K. and M. Bode (2021). Using ensemble modeling to predict the impacts of assisted migration on recipient ecosystems. *Conservation Biology* 35(2), 678–687. [10](#)
- Peterson, K. A., M. D. Barnes, C. Jeynes-Smith, S. Cowen, L. Gibson, C. Sims, C. M. Baker, and M. Bode (2021). Reconstructing lost ecosystems: A risk analysis framework for planning multispecies reintroductions under severe uncertainty. *Journal of Applied Ecology* 58(10), 2171–2184. [10](#), [18](#)
- Qiao, L., A. Khalilimeybodi, N. J. Linden-Santangeli, and P. Rangamani (2024). The evolution of systems biology and systems medicine: From mechanistic models to uncertainty quantification. *Annual Review of Biomedical Engineering* 27. [2](#)
- Rachel, L. (2024). The second wave. *Review of Economic Design*. [4](#)

- Raymond, B., J. McInnes, J. M. Dambacher, S. Way, and D. M. Bergstrom (2011). Qualitative modelling of invasive species eradication on subantarctic Macquarie Island. *Journal of Applied Ecology* 48(1), 181–191. [17](#)
- Rendall, A. R., D. R. Sutherland, C. M. Baker, B. Raymond, R. Cooke, and J. G. White (2021). Managing ecosystems in a sea of uncertainty: invasive species management and assisted colonizations. *Ecological Applications* 31(4), e02306. [10](#)
- Roemer, G. W., C. J. Donlan, and F. Courchamp (2002). Golden eagles, feral pigs, and insular carnivores: how exotic species turn native predators into prey. *Proceedings of the National Academy of Sciences* 99(2), 791–796. [4](#)
- Rohr, R. P., S. Saavedra, and J. Bascompte (2014). On the structural stability of mutualistic systems. *Science* 345(6195). [9](#)
- Saltelli, A., M. Ratto, S. Tarantola, F. Campolongo, et al. (2006). Sensitivity analysis practices: Strategies for model-based inference. *Reliability Engineering & System Safety* 91(10-11), 1109–1125. [2](#), [19](#)
- Saunders, K. R., O. Forbes, J. K. Hopf, C. R. Patterson, S. A. Vollert, K. Brown, R. Browning, M. A. Canizares, R. S. Cottrell, L. Li, et al. (2025). Data-driven recommendations for enhancing real-time natural hazard warnings. *One Earth* 8(5). [4](#)
- Sillmann, J., T. Thorarinsdottir, N. Keenlyside, N. Schaller, L. V. Alexander, G. Hegerl, S. I. Seneviratne, R. Vautard, X. Zhang, and F. W. Zwiers (2017). Understanding, modeling and predicting weather and climate extremes: Challenges and opportunities. *Weather and Climate Extremes* 18, 65–74. [2](#)
- Simpson, M. J., A. P. Browning, D. J. Warne, O. J. Maclaren, and R. E. Baker (2022). Parameter identifiability and model selection for sigmoid population growth models. *Journal of Theoretical Biology* 535, 110998. [4](#), [5](#), [30](#)
- Simpson, M. J., S. A. Walker, E. N. Studerus, S. W. McCue, R. J. Murphy, and O. J. Maclaren (2023). Profile likelihood-based parameter and predictive interval analysis guides model choice for ecological population dynamics. *Mathematical Biosciences* 355, 108950. [30](#)
- Sinha, R., C. J. Paredis, V.-C. Liang, and P. K. Khosla (2001). Modeling and simulation methods for design of engineering systems. *Journal of Computing and Information Science in Engineering* 1(1), 84–91. [2](#)
- Sisson, S. A., Y. Fan, and M. Beaumont (2018). *Handbook of approximate Bayesian computation*. CRC Press. [2](#), [3](#), [7](#), [17](#), [20](#)
- Sisson, S. A., Y. Fan, and M. M. Tanaka (2007). Sequential Monte Carlo without likelihoods. *Proceedings of the National Academy of Sciences* 104(6), 1760–1765. [40](#)
- Skataric, M. and E. D. Sontag (2012). A characterization of scale invariant responses in enzymatic networks. *PLoS Computational Biology* 8(11), e1002748. [13](#)
- Srinivasan, B. (2023). A guide to enzyme kinetics in early drug discovery. *The FEBS Journal* 290(9), 2292–2305. [14](#)
- Stessens, L., J. Gielen, R. Meeusen, and J.-M. Aerts (2024). Physical performance estimation in practice: A systematic review of advancements in performance prediction and modeling in cycling. *International Journal of Sports Science & Coaching* 19(5), 2222–2243. [4](#)
- Sundberg, M. (2012). Creating convincing simulations in astrophysics. *Science, Technology, & Human Values* 37(1), 64–87. [2](#)



- Sunnåker, M., A. G. Busetto, E. Numminen, J. Corander, M. Foll, and C. Dessimoz (2013). Approximate Bayesian computation. *PLoS Computational Biology* 9(1), e1002803. [3](#), [20](#)
- Vélez de Mendizábal, N., J. Carneiro, R. V. Solé, J. Goñi, J. Bragard, I. Martinez-Forero, S. Martinez-Pasamar, J. Sepulcre, J. Torrealdea, F. Bagnato, et al. (2011). Modeling the effector-regulatory T cell cross-regulation reveals the intrinsic character of relapses in Multiple Sclerosis. *BMC Systems Biology* 5, 1–15. [4](#)
- Vellard, M. (2003). The enzyme as drug: application of enzymes as pharmaceuticals. *Current Opinion in Biotechnology* 14(4), 444–450. [14](#)
- Vilas, M. P., F. Egger, M. P. Adams, H. R. Maier, B. Robson, J. F. Mestres, L. Stewart, P. Maxwell, and K. R. O’Brien (2023). TALKS: A systematic framework for resolving model-data discrepancies. *Environmental Modelling & Software* 163, 105668. [19](#)
- Villaverde, A. F. and J. R. Banga (2014). Reverse engineering and identification in systems biology: strategies, perspectives and challenges. *Journal of the Royal Society Interface* 11(91), 20130505. [2](#)
- Vollert, S. A., C. Drovandi, and M. P. Adams (2024). Unlocking ensemble ecosystem modelling for large and complex networks. *PLoS Computational Biology* 20(3), e1011976. [10](#), [11](#), [17](#), [33](#)
- Vollert, S. A., C. Drovandi, and M. P. Adams (2025). Ecosystem knowledge should replace coexistence and stability assumptions in ecological network modelling. *Bulletin of Mathematical Biology* 87(1), 17. [3](#), [4](#), [10](#), [17](#)
- Warne, D. J., K. Crossman, G. E. Heron, J. A. Sharp, W. Jin, P. P.-Y. Wu, M. J. Simpson, K. Mengersen, and J.-C. Ortiz (2024). Mathematical modelling and uncertainty quantification for analysis of biphasic coral reef recovery patterns. *arXiv preprint arXiv:2406.19591*. [16](#)
- Warne, D. J., K. A. Crossman, W. Jin, K. Mengersen, K. Osborne, M. J. Simpson, A. A. Thompson, P. Wu, and J.-C. Ortiz (2022). Identification of two-phase recovery for interpretation of coral reef monitoring data. *Journal of Applied Ecology* 59(1), 153–164. [16](#)
- Wellmann, F. and G. Caumon (2018). 3-D structural geological models: Concepts, methods, and uncertainties. In *Advances in Geophysics*, Volume 59, pp. 1–121. Elsevier. [2](#)
- Wesner, J. S. and J. P. Pomeranz (2021). Choosing priors in Bayesian ecological models by simulating from the prior predictive distribution. *Ecosphere* 12(9), e03739. [18](#)



## Supplementary materials

### S.1 Additional modelling details for each of the case studies

This work demonstrates the value of using non-empirical information within model calibration for mechanistic models. To demonstrate our methods, we will use three different modelling examples: a case study of logistic coral growth calibrated with expert-elicited knowledge, a case study of ecosystem population modelling calibrated using ubiquitous theories of long-term population dynamics, and a case study of biochemical reaction networks calibrated to be adaptive to changes in input. In this section, we provide additional details of the modelling scenarios that may be necessary to replicate our study.

#### S.1.1 Case study 1: Logistic coral growth

Section 2.1, [Case study 1: Logistic coral growth](#) in the main text describes a simple modelling scenario, where the percentage of coral cover on a reef following a disturbance is described using a logistic model. In this example, the percentage of coral cover on a reef can be modelled as

$$\frac{dy}{dt} = ry(t) \left( 1 - \frac{y(t)}{K} \right), \quad y(0) = y_0, \quad (\text{S1})$$

where  $y$  is the coral cover (% area),  $t$  is the time (years),  $r$  is a growth rate parameter ( $\text{year}^{-1}$ ),  $K$  is the carrying capacity (% area), and  $y_0$  is the initial coral cover (% area). This ordinary differential equation can be solved analytically as

$$y(t) = \frac{Ky_0}{y_0 + (K - y_0)e^{-rt}}. \quad (\text{S2})$$

This model has three model parameters to be calibrated (Table S1). Since this is an illustrative example, the specified prior distributions are arbitrary, however, the bounds are loosely based on other works in the literature ([Simpson et al., 2022, 2023](#)).

Parameter	Description	Units	Prior distribution
$r$	Growth rate	1/year	$U(0, 0.5)$
$K$	Maximum coral cover	% area	$U(60, 80)$
$y_0$	initial coral cover	% area	$U(0, 5)$

Table S1: The model parameters associated with the logistic growth model used in Section 2.1, [Case study 1: Logistic coral growth](#).

Two non-empirical constraints were considered. Firstly, we constrain acceptable parameter sets by requiring slow initial growth, such that coral cover should be less than 10% within the first 5 years. Secondly, acceptable parameter sets must exhibit recovery, such that coral populations should be within 1% percentage area of carrying capacity within 50 years. Both of these statements correspond to a summary statistic, that is expected to be within some bounds. Here, these conditions can be expressed as

$$y(5) = \frac{Ky_0}{y_0 + (K - y_0)e^{-5r}} \leq 10\%, \quad (\text{S3})$$

$$y(50) = \frac{Ky_0}{y_0 + (K - y_0)e^{-50r}} \geq K - 1\%, \quad (\text{S4})$$

such that  $y(5)$  and  $y(50)$  are summary statistics in the model. These summary statistics can then be easily compared to the expert knowledge via one discrepancy function  $\rho$ :

$$\rho = \rho_5 + \rho_{50}, \quad (\text{S5})$$

$$\rho_5 = \max(0, y(5) - 10), \quad (\text{S6})$$

$$\rho_{50} = \max(0, K - 1 - y(50)), \quad (\text{S7})$$

where  $\rho_5$  measures the discrepancy of coral cover exceeding 10% in the first 5 years,  $\rho_{50}$  measures the discrepancy of coral cover not recovering within 1% of  $K$  in 50 years, and  $\rho$  measures the total discrepancy between the simulated and expected coral cover.

In addition, we generated three sparse observations of coral cover (Table S2) to demonstrate how data can be used within our framework.

Time (years)	Coral cover (% area)
1	4
3	4
10	10

Table S2: The time-series dataset used to calibrate the logistic growth model in Section 2.1, [Case study 1: Logistic coral growth](#).

To calibrate the model to this dataset we used a Gaussian likelihood, which assumes normally distributed measurement noise.

$$f(\mathbf{y}_{\text{obs}}|\boldsymbol{\theta}) = \prod_{i=1}^n f(y_{\text{obs},i}|\boldsymbol{\theta}) \quad (\text{S8})$$

$$= \prod_{i=1}^n \frac{1}{\sqrt{2\pi}\sigma} \exp\left(-\frac{y_{\text{sim},i}(\boldsymbol{\theta}) - y_{\text{obs},i}}{2\sigma^2}\right) \quad (\text{S9})$$

where  $f(\mathbf{y}_{\text{obs}}|\boldsymbol{\theta})$  is the likelihood of observing data  $\mathbf{y}_{\text{obs}}$  from a model characterised by parameters  $\boldsymbol{\theta}$ ,  $n$  is the number of observed data points,  $y_{\text{obs},i}$  is the  $i$ th observation,  $\sigma$  is a parameter representing measurement noise, and  $y_{\text{sim},i}$  is the data simulated by the model characterised by parameters  $\boldsymbol{\theta}$  with equivalent inputs to that of data point  $i$ . Hence, for the data described in Table S2,  $n = 3$ ,  $\mathbf{y}_{\text{obs}} = \{4, 4, 10\}$ , and  $\mathbf{y}_{\text{sim}} = \{y(1), y(3), y(10)\}$ .

We generated 10000 parameter sets for each of the target distributions using our sequential Monte Carlo (SMC) algorithm that blends exact and approximate approaches. Details on this sampling algorithm can be found in Supplementary Material Section S.3.

### S.1.2 Case study 2: Ecosystem population modelling

Section 2.2, [Case study 2: Ecosystem population modelling](#) in the main text describes an ecosystem population model, used to model the populations of four interacting species for making management decisions. In this paper, we focus on modelling the network depicted in Figure 4A, comprised of foxes ( $F$ ), rabbits ( $R$ ), small mammals ( $M$ ) and vegetation ( $V$ ). We use the generalised Lotka-Volterra equations to model this network as a system of ordinary differential equations, which is used to model population predictions in an ecosystem as

$$\frac{dn_i}{dt} = \left[ r_i + \sum_{j=1}^N \alpha_{i,j} n_j(t) \right] n_i(t), \quad (\text{S10})$$

where  $n_i(t)$  is the abundance of the  $i$ th species at time  $t$ ,  $r_i$  is the growth rate of the  $i$ th species,  $N$  is the number of species being modelled, and  $\alpha_{i,j}$  is the per-capita interaction strength characterising the effect of species  $j$  on species  $i$ . The presence and sign of interactions between species  $\alpha_{i,j}$  are prescribed by the ecosystem network (e.g., fox populations negatively affect rabbit populations therefore  $\alpha_{R,F} < 0$ , but fox populations have no direct effect on vegetation abundance so  $\alpha_{V,F} = 0$ ).

For the network we consider, the full Lotka-Volterra ecosystem model can be written as

$$\frac{dn_F}{dt} = [r_F + \alpha_{F,F}n_F(t) + \alpha_{F,R}n_R(t) + \alpha_{F,M}n_M(t)]n_F(t), \quad (\text{S11})$$

$$\frac{dn_R}{dt} = [r_R + \alpha_{R,F}n_F(t) + \alpha_{R,R}n_R(t) + \alpha_{R,V}n_V(t)]n_R(t), \quad (\text{S12})$$

$$\frac{dn_M}{dt} = [r_M + \alpha_{M,F}n_F(t) + \alpha_{M,M}n_M(t) + \alpha_{M,V}n_V(t)]n_M(t), \quad (\text{S13})$$

$$\frac{dn_V}{dt} = [r_V + \alpha_{V,R}n_R(t) + \alpha_{V,M}n_M(t) + \alpha_{V,V}n_V(t)]n_V(t). \quad (\text{S14})$$

Alternatively, we can express this model in vector form, such that

$$\frac{d\mathbf{n}}{dt} = [\mathbf{r} + \mathbf{A}\mathbf{n}] \circ \mathbf{n}, \quad (\text{S15})$$

where  $\mathbf{n} = \{n_i : i = F, R, M, V\}$  is a vector of populations for each species,  $\mathbf{r} = \{r_i : i = F, R, M, V\}$  is the vector of growth rates for each group,  $\mathbf{A} = \{\alpha_{i,j} : i, j = F, R, M, V\}$  is the  $N \times N$  interaction matrix of per-capita interaction strengths between ecosystem nodes,  $\circ$  is the Hadamard or element-wise product, and the subscripts  $F, R, M$ , and  $V$  refer to foxes, rabbits, small mammals and vegetation, respectively.

To solve this system of ordinary differential equations, we additionally require initial populations for each of the species  $n_i(0)$  where  $i = \{F, R, M, V\}$ . As such, 16 parameters in this model require calibration (see Table S3).

Parameter	Description	Prior
$n_F(0)$	Initial fox population	$U(0.25, 1)$
$n_R(0)$	Initial rabbit population	$U(0.5, 1)$
$n_M(0)$	Initial small mammal population	$U(0, 1)$
$n_V(0)$	Initial vegetation population	$U(0.25, 1)$
$r_F, r_R, r_M$ , and $r_V$	Species growth rates	$U(-1, 1)$
$\alpha_{F,F}, \alpha_{R,R}, \alpha_{M,M}$ , and $\alpha_{V,V}$	Intra-species interaction	$U(-1, 0)$
$\alpha_{R,F}, \alpha_{M,F}, \alpha_{V,R}$ , and $\alpha_{V,M}$	Negative species interaction	$U(-1, 0)$
$\alpha_{F,R}, \alpha_{F,M}, \alpha_{R,V}$ , and $\alpha_{M,V}$	Positive species interaction	$U(0, 1)$

Table S3: The model parameters associated with the logistic growth model used in Section 2.1, Case study 1: Logistic coral growth.

In this ecosystem example, we consider two non-empirical constraints: equilibrium feasibility and stability. *Feasibility* (often referred to as coexistence) specifically measures whether the equilibrium populations of each population are positive (Grilli et al., 2017), where the equilibrium populations are calculated as

$$\mathbf{n}^* = -\mathbf{A}^{-1}\mathbf{r} > \mathbf{0}, \quad (\text{S16})$$

where  $\mathbf{n}^*$  is the vector of equilibrium population abundances for all species  $n_i^* = \{i : C, R, B, V\}$ . These four equilibrium abundances are each summary statistics that must all be positive to meet the feasibility condition.

*Stability* measures the ability of the equilibrium to resist changes from small external pressures (Allesina and Tang, 2012) and is measured by taking the eigenvalues  $\lambda$  of the Jacobian matrix  $\mathbf{J}$  evaluated at equilibrium  $\mathbf{n}^*$ . For Lotka-Volterra each element  $(i, j)$  of the Jacobian  $\mathbf{J}$  is calculated as  $J_{i,j} = \alpha_{i,j}n_i^*$ ,  $\forall i, j$  in  $\{F, R, M, V\}$  such that the summary statistics for stability are real components of the four eigenvalues

$$\mathbb{R}(\lambda) < 0 \quad (\text{S17})$$

of the Jacobian matrix  $\mathbf{J}$  and must each be negative for a stable equilibrium. For a more detailed explanation of the calculation of these summary statistics see Vollert et al. (2024). All eight summary statistics (four equilibrium abundances  $n_i^*$  for each species  $i = \{F, R, M, V\}$ , and four real components of eigenvalues  $\mathbb{R}(\lambda_i)$  for each dimension in the population-space) are then combined within a single discrepancy, calculated as

$$\rho = \sum_{i=1}^4 |\min\{0, n_i^*\}| + \sum_{i=1}^4 |\max\{0, \mathbb{R}(\lambda_i)\}|, \quad (\text{S18})$$

such that  $\rho$  measures the discrepancy in equilibrium behaviour from the theorised feasible and stable behaviour.

In addition to calibrating this model with non-empirical constraints, we calibrate the model to a simulated time-series dataset of nine observations per species (see Table S4).

Time	Populations			
	Fox	Rabbit	Small mammal	Vegetation
0	0.4641	0.6850	0.8673	0.7174
1	0.5877	0.7865	0.5226	0.6179
2	1.0489	1.0748	0.3640	0.4555
3	1.4754	0.8941	0.1997	0.5363
4	1.7064	0.7186	0.2047	0.4482
5	1.6375	0.7417	0.1703	0.6880
6	1.4619	0.6292	0.1371	0.8902
7	1.6266	0.6306	0.2197	1.1218
8	1.4009	0.8132	0.0883	1.1005

Table S4: The time-series dataset used to calibrate the ecosystem population model in Section 2.2, Case study 2: Ecosystem population modelling.

We used a Gaussian likelihood to calibrate the model to this dataset (see Equation (13)), which assumes normally distributed measurement noise. Specifically, for ecosystem population modelling, the likelihood function was defined as

$$f(\mathbf{y}_{\text{obs}}|\boldsymbol{\theta}) = \prod_{i=1}^N \prod_{j=1}^D \frac{1}{\sqrt{2\pi}\sigma_i} \exp\left(-\frac{y_{\text{sim},i}(t_j, \boldsymbol{\theta}) - y_{\text{obs},i}(t_j)}{2\sigma_i^2}\right) \quad (\text{S19})$$

where  $f(\mathbf{y}_{\text{obs}}|\boldsymbol{\theta})$  is the likelihood of observing data  $\mathbf{y}_{\text{obs}}$  (Table S4) from a model characterised by parameters  $\boldsymbol{\theta}$ ,  $N$  is the number of species which is 4 for this system,  $D$  is the number of observations per species which is 9 for this system,  $\sigma_i$  is a parameter representing measurement noise for species  $i$ ,  $y_{\text{obs},i}(t_j)$  is the  $j$ th observation of species  $i$ , and  $y_{\text{sim},i}(t_j)$  is the data simulated by the model characterised by parameters  $\boldsymbol{\theta}$  for species  $i$  at the time point of the  $j$ th observation.

We generated 100000 parameter sets for each of the target distributions using our SMC algorithm that blends exact and approximate approaches. Details on this sampling algorithm can be found in Supplementary Material Section S.3.

### S.1.3 Case study 3: Biochemical adaptation

Section 2.3, [Case study 3: Biochemical adaptation](#) in the main text describes a biochemical reaction network used to model a system of interacting protein substrates ( $A$  and  $B$ ), their activated forms ( $A^*$  and  $B^*$ ), enzymes ( $E_1$  and  $E_4$ ), and intermediate protein-protein complexes ( $C_1 = [AE_1]$ ,  $C_2 = [A^*B^*]$ ,  $C_3 = [A^*B]$  and  $C_4 = [B^*E_4]$ ). In this paper, we use a general modelling framework known as the ‘complex complete framework’, which explicitly accounts for the formation of intermediate complexes. The system of biochemical reactions depicted in Figure 6A is described by the following ten ordinary differential equations ([Jeynes-Smith and Araujo, 2023](#)):

$$\frac{dA}{dt} = d_1C_1 + k_2C_2 - a_1AE_1, \quad (\text{S20})$$

$$\frac{dA^*}{dt} = k_1C_1 + d_2C_2 + d_3C_3 + k_3C_3 - a_3A^*B - a_2A^*B^*, \quad (\text{S21})$$

$$\frac{dB}{dt} = d_3C_3 + k_4C_4 - a_3BA^*, \quad (\text{S22})$$

$$\frac{dB^*}{dt} = d_2C_2 + k_2C_2 + d_4C_4 + k_3C_3 - a_2A^*B^* - a_4B^*E_4, \quad (\text{S23})$$

$$\frac{dE_1}{dt} = (d_1 + k_1)C_1 - a_1AE_1, \quad (\text{S24})$$

$$\frac{dE_4}{dt} = (d_4 + k_4)C_4 - a_4B^*E_4, \quad (\text{S25})$$

$$\frac{dC_1}{dt} = a_1AE_1 - (d_1 + k_1)C_1, \quad (\text{S26})$$

$$\frac{dC_2}{dt} = a_2A^*B^* - (d_2 + k_2)C_2, \quad (\text{S27})$$

$$\frac{dC_3}{dt} = a_3A^*B - (d_3 + k_3)C_3, \quad (\text{S28})$$

$$\frac{dC_4}{dt} = a_4B^*E_4 - (d_4 + k_4)C_4. \quad (\text{S29})$$

Here,  $t$  is time,  $a_i$  are the association rate constants,  $d_i$  are the dissociation rate constants, and  $k_i$  are the catalytic rate constants for  $i = \{1, 2, 3, 4\}$ . For this study we fix parameters related to the total substrate  $A_{\text{TOT}} = A + A^* + C_1 + C_2 + C_3 = 10$  and  $B_{\text{TOT}} = B + B^* + C_2 + C_3 + C_4 = 10$ . All 12 parameters in the model are highly uncertain and require calibration (see Table S5). For more information on this model and its parameters, see [Jeynes-Smith and Araujo \(2023\)](#).

Parameter	Description	Prior
$a_i$ for $i = \{1, 2, 3, 4\}$	Association rates	$\log a_i \sim \mathcal{U}(-3, 4)$
$d_i$ for $i = \{1, 2, 3, 4\}$	Dissociation rates	$\log d_i \sim \mathcal{U}(-3, 4)$
$k_i$ for $i = \{1, 2, 3, 4\}$	Catalytic rates	$\log k_i \sim \mathcal{U}(-3, 4)$

Table S5: The model parameters associated with the biochemical network model used in Section 2.3, [Case study 3: Biochemical adaptation](#).

To solve this system of ordinary differential equations, we simulate the system specified by the initial conditions in Table S6 for  $t = 0$  to  $t = 10^6$  and assume that the model has reached a steady state after this time. Then, the system is perturbed by increasing the concentration of  $E_1$  by 1, and the system is again solved for a period of  $10^2$ .

Initial condition	Value
$A(0)$	10
$A^*(0)$	0
$B(0)$	10
$B^*(0)$	0
$E_1(0)$	1
$E_4(0)$	1
$C_1(0)$	0
$C_2(0)$	0
$C_3(0)$	0
$C_4(0)$	0

Table S6: Initial condition parameter values assumed in the biochemical network model used in Section 2.3, [Case study 3: Biochemical adaptation](#).

For the system to be considered adaptive, two conditions must be met after it is stimulated: *sensitivity* and *precision* ([Ma et al., 2009](#)). Sensitivity,  $S$ , measures the ability for a chemical concentration,  $O$ , to react to a change in stimulus,  $I$ ,

$$S = \frac{|O_{\text{peak}} - O_1|/O_1}{|I_2 - I_1|/I_1}, \quad (\text{S30})$$

where  $O_1$  and  $I_1$  are the original chemical concentrations (output) and stimulus (input), respectively,  $I_2$  is the updated stimulus, and  $O_{\text{peak}}$  is the concentration of  $O$  which is furthest from  $O_1$  after altering the stimulus (see Figure 6B). A biochemical network that is sensitive to changes in input will have  $S > 1$  ([Ma et al., 2009](#)).

The precision,  $P$ , is a measure of how well the system can return to its original value,

$$P = \left( \frac{|O_2 - O_1|/O_1}{|I_2 - I_1|/I_1} \right)^{-1}, \quad (\text{S31})$$

where  $O_2$  is the final chemical concentration (output) after being stimulated. A biochemical network is considered precise if  $P > 10$  ([Ma et al., 2009](#)). Hence, we can define the discrepancy between adaptive biochemical networks and a model simulation as

$$\rho = \max(0, 1 - S) + \max(0, 10 - P) \quad (\text{S32})$$

such that  $\rho$  measures the discrepancy in sensitivity and precision for some stimulus.

We generated 10000 parameter sets that led to sensitive and precise biochemical systems using an SMC-ABC sampler ([Drovandi and Pettitt, 2011](#)). Of the 10000 parameter sets drawn naively from the prior distribution 0.18% of these satisfied the precision and sensitivity requirements.

In this case study, we are particularly interested in the Michaelis-Menten constants  $K_3$  and  $K_4$  which relate to the binding affinity of the complexes  $C_3$  and  $C_4$ . These Michaelis constants are calculated using the association, dissociation and catalytic rates as

$$K_i = (d_i + k_i)/a_i, \quad (\text{S33})$$

where  $K_i$  is the  $i$ th Michaelis-Menten constant. Previous literature indicates that for this biochemical network to be capable of adaptation, both  $K_3 < 1$  and  $K_4 < 1$  ([Ma et al., 2009](#); [Jeynes-Smith and Araujo, 2023](#)).

## S.2 Additional results for each of the case studies

### S.2.1 Case study 1: Logistic coral growth

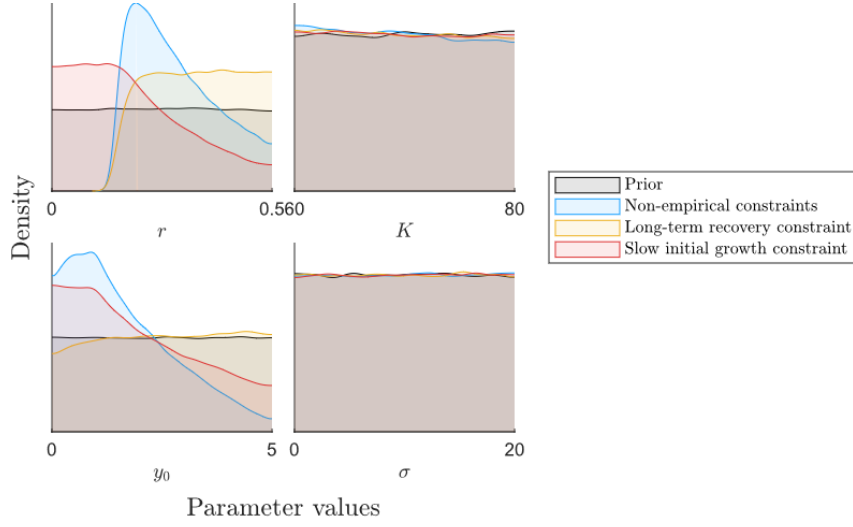


Figure S1: The marginal distributions of each model parameter for the logistic growth example from the prior, both non-empirical constraints individually and in combination. Notice that the distribution of the combination of two non-empirical constraints, is not necessarily the overlap between distributions.



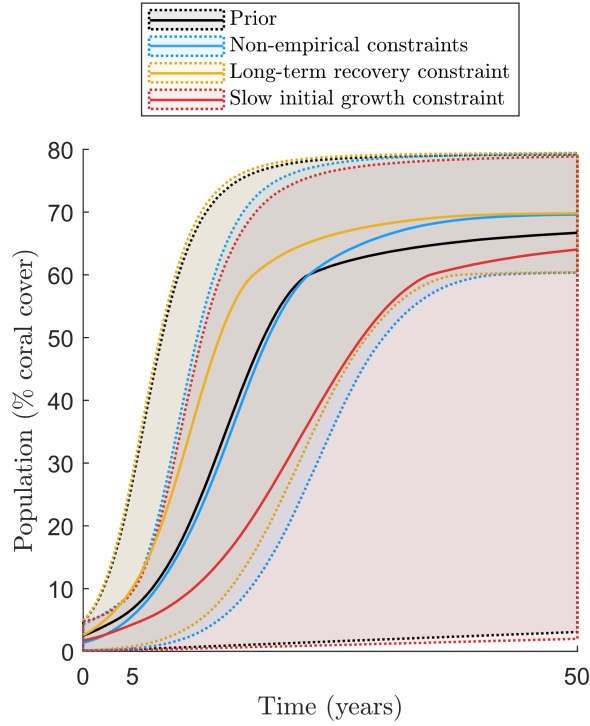


Figure S2: Model forecasts generated using ensembles of model parameters from the prior distribution (grey), the distribution with slow initial coral growth (red), the distribution with long-term coral recovery (yellow), and the distribution with both constrained (blue). Here we show the median prediction and the 95% credible intervals. Notice that constraining the coral cover at 5 years mostly affects the earlier stages of predictions, and the constraint on 50-year coral cover mostly affects the late-stage predictions. Additionally, the overlap in predictions for each individual constraint matches the predictions from the joint distribution.

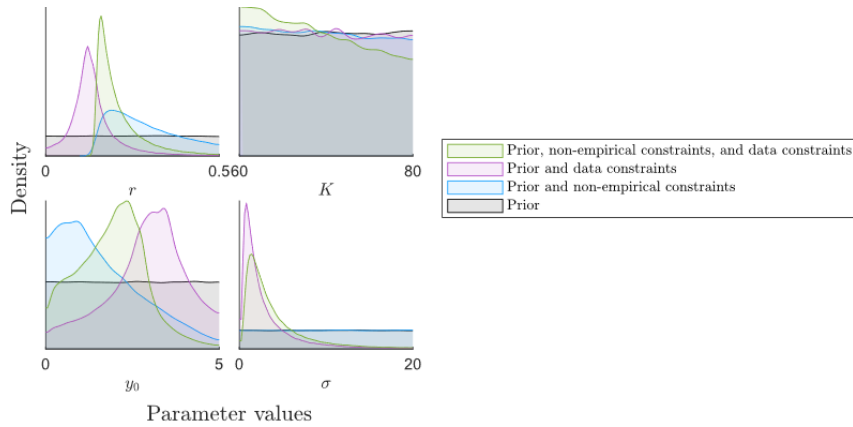


Figure S3: The marginal distributions of each model parameter for the logistic growth example from the prior, constraint posterior, data posterior, and constraint and data posterior distributions.

### S.2.2 Case study 2: Ecosystem population modelling

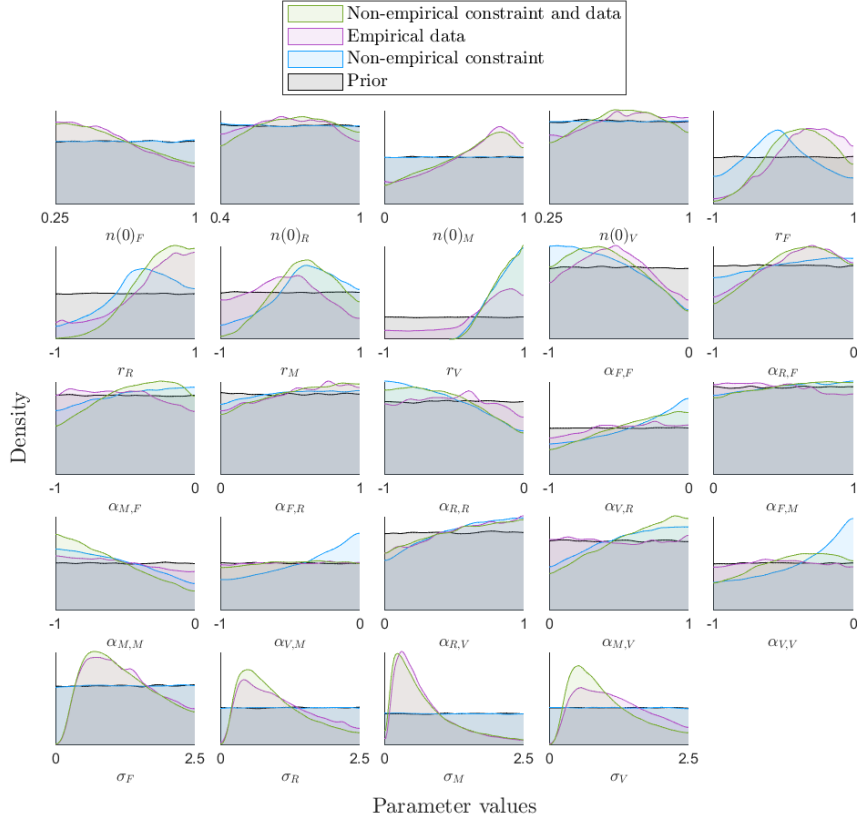


Figure S4: Marginal parameter distributions for each model parameter in the ecosystem population model. Four distributions of parameters are shown for the prior (grey), equilibrium-constrained posterior (blue), time-series data posterior (purple) and the combined equilibrium-constrained and time-series data posterior (green). Notice that the parameters most informed by the data are related to the Gaussian measurement noise  $\sigma$ . Whereas, the constraints on stability and coexistence yield far more informed parameter inferences.

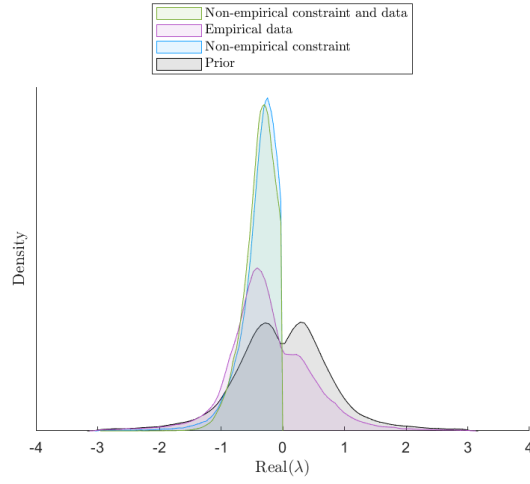


Figure S5: Distributions indicating the stability of the ecosystem population model. For each distribution of parameter sets, we show the distribution of the real parts of the eigenvalues of the Jacobian matrix evaluated at equilibrium, where negative values indicate stability. Four distributions are shown for the prior (grey), equilibrium-constrained posterior (blue), time-series data posterior (purple) and the combined equilibrium-constrained and time-series data posterior (green). Notice that all distributions where stability is enforced are strictly negative (blue and green), and when informed by a dataset the system is more likely to be stable (purple) than when the data is not considered (grey).

### S.2.3 Case study 3: Biochemical adaptation

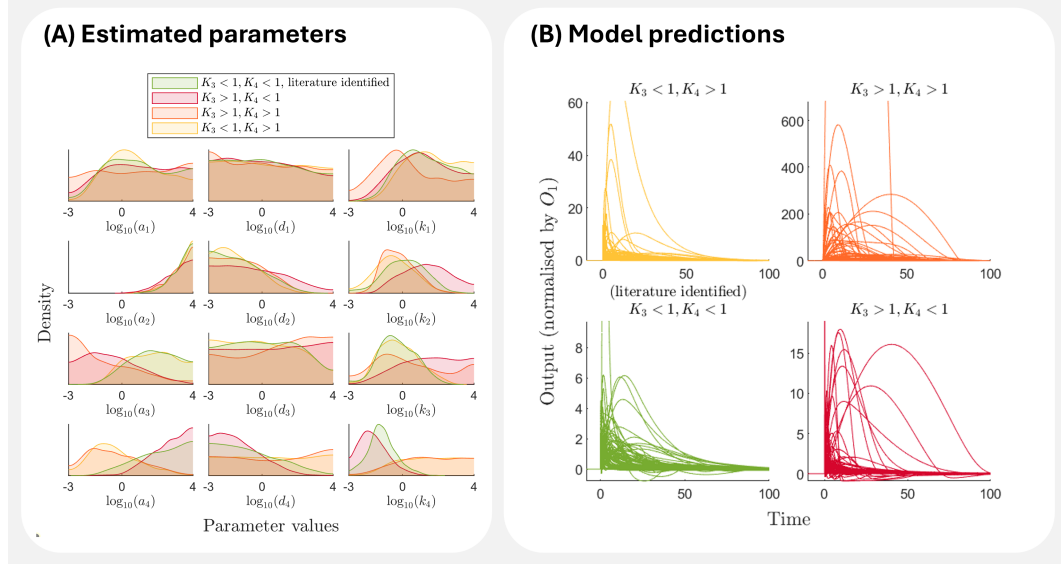


Figure S6: The parameter sets capable of adaptation, categorised according to their Michaelis-Menten constants  $K_3$  and  $K_4$  (see Figure 7 bottom left plot for these categories). (A) The estimated marginal parameter distributions for each of the Michaelis-Menten groups. (B) Model predictions for 100 randomly selected parameter sets from each Michaelis-Menten group. Notice that both distributions and predictions for the literature-identified subgroup (green;  $K_3 < 1, K_4 < 1$ ) are not distinct from the others, and that all plotted parameter sets meet the criteria of sensitive and precise adaptation.

### S.3 Sampling algorithm

Bayesian sampling algorithms aim to obtain a sample of parameter sets that is representative of the distribution being targeted (Martin et al., 2024). Sequential Monte Carlo (SMC) is one such sampling algorithm frequently used to obtain a sample from the posterior (Del Moral et al., 2006) or the approximate posterior distribution (Sisson et al., 2007). SMC is a generally reliable sampling algorithm, and in particular, it is robust to the shape of the target distribution, minimises convergence issues, and is efficient when acceptance rates are low or the number of parameters is high (Sisson et al., 2007).

The general idea of an SMC algorithm is that an ensemble of weighted parameter sets is moved through a sequence of distributions, starting from the prior and ending at the target distribution, breaking the sampling problem into a series of simpler problems (Del Moral et al., 2006). For every sequence in the distribution, three steps are repeated – reweighting, resampling, and moving – until the final target distribution is obtained (Jeremiah et al., 2012; Chopin, 2002; Beaumont, 2019).

1. **Reweighting:** Select a new intermediate target distribution and weight each parameter set using the probability of obtaining it from this distribution.
2. **Resampling:** Duplicate and eliminate parameter sets depending on their weight.
3. **Moving:** Adjust the parameter values according to the intermediate target distribution via MCMC (Gaman and Lopes, 2006).

When applied to a dataset, a likelihood function is used to weight the parameter sets, and a common choice for the sequence of distributions is likelihood annealing, whereby the intermediate target distributions are proportional to  $\pi(\boldsymbol{\theta})f(\mathbf{y}_{\text{obs}}|\boldsymbol{\theta})^\gamma$  where  $\gamma$  is increased from 0 (prior distribution) to 1 (posterior). The effective sample size (ESS) is typically used when selecting  $\gamma$  to ensure that not all of the weight is on very few parameter sets (Jasra et al., 2011). Similarly, for SMC-ABC, a discrepancy function is used to weight the parameter sets such that the intermediate target distributions are selected to iteratively reduce the discrepancy threshold  $\epsilon$ , where a common choice is to update the discrepancy threshold  $\epsilon$  such that some percentage of parameter sets are below it (Drovandi and Pettitt, 2011).

However, when targeting a distribution that includes both a likelihood and a discrepancy function (Equation (14)), the weights on the parameter set need to be made up of both functions. Algorithm S1 describes our SMC algorithm that simultaneously anneals both the likelihood and discrepancy information, where any changes from a standard SMC algorithm that only incorporates the likelihood are shown in blue. In this algorithm, the intermediate target distribution is determined by first selecting a new discrepancy threshold such that  $a\%$  of parameter sets with the lowest discrepancy are retained, and all parameter sets with higher discrepancy are given zero weight. Then, the likelihood annealing temperature  $\gamma$  is chosen using the updated weights, such that the influence of the likelihood is as high as possible, without dropping the effective sample size below some limit.

In Algorithm S1, the tuning parameters used throughout this study were specified as  $a = 0.6$ ,  $ESS_{\min} = 0.3$ ,  $c = 0.99$ ,  $n_{\text{MCMC}} = 10$ .

---

**Algorithm S1:** SMC algorithm which incorporates both a likelihood and a discrepancy function. Differences from a standard SMC algorithm that only incorporates the likelihood are highlighted in blue.

---

#### INITIALISE

Import the dataset,  $\mathbf{y}_{\text{obs}}$   
Specify the prior distribution,  $\pi(\boldsymbol{\theta})$   
Specify the likelihood function,  $f(\mathbf{y}_{\text{obs}}|\boldsymbol{\theta})$   
Specify the discrepancy function,  $\rho(\mathbf{S}_{\text{obs}}, \mathbf{S}_{\text{sim}}|\boldsymbol{\theta})$   
Specify the target discrepancy threshold,  $\epsilon$   
Select the SMC tuning variables including:  
    The number of particles to be sampled,  $n$   
    The percentage of particles with the lowest discrepancy to be retained at each step,  $a$   
    The minimum acceptable ESS before resampling must occur,  $\text{ESS}_{\min}$ , where  
     $\text{ESS}_{\min} < a \times n$   
    The desired probability of particles moved during each MCMC step,  $c$   
    The number of trial MCMC-ABC steps to gauge acceptance rate,  $n_{\text{MCMC}}$

Generate a sample of  $n$  particles ( $\{\boldsymbol{\theta}_i\}_{i=1}^n$ ) from the prior distribution,  $\pi(\boldsymbol{\theta})$   
Set the particle weights ( $\{W_i^t\}_{i=1}^n$ ) to be equal, such that  $W_i^t = 1/n$   
Simulate the model for each  $\{\boldsymbol{\theta}_i\}_{i=1}^n$ , to calculate the log-likelihood  $\log f(\mathbf{y}_{\text{obs}}|\boldsymbol{\theta}_i)$  and  
discrepancy  $\rho(\mathbf{S}_{\text{obs}}, \mathbf{S}_{\text{sim}}|\boldsymbol{\theta}_i)$  of each particle  $i$   
Initialise the temperature for likelihood annealing,  $\gamma_t = 0$   
Calculate the maximum particle discrepancy,  $\rho_{\max} = \max\{\rho(\mathbf{S}_{\text{obs}}, \mathbf{S}_{\text{sim}}|\boldsymbol{\theta}_i)\}_{i=1}^n$

**while** the discrepancy threshold is exceeded,  $\rho_{\max} > \epsilon$ , **OR** the target distribution is not yet at the posterior,  $\gamma_t < 1$  **do**

Sort the particles by their discrepancy,  $\rho(\mathbf{S}_{\text{obs}}, \mathbf{S}_{\text{sim}}|\boldsymbol{\theta})$   
Select the discrepancy threshold  $\epsilon_t = \rho(\mathbf{S}_{\text{obs}}, \mathbf{S}_{\text{sim}}|\boldsymbol{\theta}_{a \times n})$   
Set the weights to 0 for particles with discrepancy above  $\epsilon_t$ , effectively removing those particles  
Select the next temperature in the sequence,  $\gamma_t$ :  
    **if** the posterior distribution ( $\gamma_t = 1$ ) has an acceptable sample size ( $\geq \text{ESS}_{\min}$ ),  
    **then** set  $\gamma_t = 1$ .  
    **else**, using the updated weights  $\{W_i^t\}_{i=1}^n$ , find the temperature at which  
     $\text{ESS}_t(\gamma_t) = \text{ESS}_{\min}$  where  $\gamma_{t-1} < \gamma_t < 1$  using the bisection method

**REWEIGHT**

Reweight the sample to fit the current distribution, such that  $w_i^t = W_i^{t-1} f(\mathbf{y}_{\text{obs}}|\boldsymbol{\theta}_i)^{\gamma_t - \gamma_{t-1}}$   
Normalise the weights,  $W_i^t = w_i^t / \sum_{k=1}^n w_k^t$   
Calculate the current ESS,  $\text{ESS}_t = 1 / \sum_{i=1}^n (W_i^t)^2$

**RESAMPLE**

Resample particle values with probabilities given by their weights,  $W_i^t$   
Reset the particle weights  $W$  such that  $W_i^t = 1/n$   
Calculate the sample covariance matrix,  $\text{cov}(\{\boldsymbol{\theta}_i\}_{i=1}^n)$ , to be used in the MCMC proposal distribution,  $q_t$

**MOVE**

**for** each of the  $n_{\text{MCMC}}$  trial MCMC steps **do**  
    Move the particles using MCMC (Algorithm S2)  
Estimate the MCMC acceptance rate for iteration  $t$ ,  $a_t$   
Determine the number of MCMC iterations to perform,  $R_t = \lceil \log(c) / \log(1 - a_t) \rceil$  and  
update  $n_{\text{MCMC}} = \lceil R_t / 2 \rceil$   
**for** each of the remaining MCMC steps,  $R_t - n_{\text{MCMC}}$  **do**  
    Move the particles using MCMC (Algorithm S2)

Update the maximum particle discrepancy,  $\rho_{\max}$

---

---

**Algorithm S2:** MCMC algorithm which incorporates both a likelihood and a discrepancy function used within the SMC algorithm (Algorithm S1). Differences from a standard MCMC algorithm that only incorporates the likelihood are highlighted in blue.

---

**for** *each particle*  $i$  *in*  $\{\boldsymbol{\theta}_i\}_{i=1}^n$  **do**

- Propose a new set of parameter values  $\boldsymbol{\theta}_i^*$  using a multivariate normal proposal distribution,  $\boldsymbol{\theta}_i^* \sim N(\boldsymbol{\theta}_i, \text{cov}(\{\boldsymbol{\theta}_i\}_{i=1}^n))$
- Accept or reject the proposed particle value based on a Metropolis-Hastings acceptance probability,  $\alpha = \min\left(1, \frac{\pi(\boldsymbol{\theta}_i^*)f(\mathbf{y}_{\text{obs}}|\boldsymbol{\theta}_i^*)^{\gamma_t} \mathbb{I}(\rho(\mathbf{S}_{\text{obs}}, \mathbf{S}_{\text{sim}}|\boldsymbol{\theta}_i^*) < \epsilon_t)}{\pi(\boldsymbol{\theta}_i)f(\mathbf{y}_{\text{obs}}|\boldsymbol{\theta}_i)^{\gamma_t} \mathbb{I}(\rho(\mathbf{S}_{\text{obs}}, \mathbf{S}_{\text{sim}}|\boldsymbol{\theta}_i) < \epsilon_t)}\right)$

Assess the portion of mutated particles

---